Pro gradu -tutkielma
Fysiikka

Wetting Characterization by Driven Ferrofluid Droplet Oscillations

Anna Liski
2018

Supervisors: Mika Latikka
Robin Ras
Examiners: Robin Ras
Simo Huotari

HELSINGIN YLIOPISTO
FYSIIKAN LAITOS

PL 64 (Gustaf Hällströmin katu 2)
00014 Helsingin yliopisto

HELSINGIN YLIOPISTO
HELSINGFORS UNIVERSITET
UNIVERSITY OF HELSINKI
MATEMAATTIS-LUONNONTIETEELLINEN TIEDEKUNTA
MATEMATISK-NATURVETENSKAPLIGA FAKULTETEN
FACULTY OF SCIENCE

Tiedekunta – Fakultet – Faculty	Koulutusohjelma – Utbildningsprogram – Degree programme
Faculty of Science	Degree Programme in Physical Sciences

Tekijä – Författare – Author

Anna Liski

Työn nimi – Arbetets titel – Title

Wetting Characterization by Driven Ferrofluid Droplet Oscillations

Työn laji – Arbetets art – Level	Aika – Datum – Month and year	Sivumäärä – Sidoantal – Number of pages
Master's Thesis	March 2018	57

Tiivistelmä – Referat – Abstract

The field of superhydrophobicity i.e. extreme water-repellency is a fast growing one ever since artificial ways of manufacturing such surfaces have been developed. Superhydrophobic surfaces have several potential applications including surfaces that are self-cleaning, corrosion and stain resistant, anti-fogging and anti-fouling. For the use of superhydrophobic surfaces in applications there is a need for a precise characterization of their wetting properties. However, conventional methods for characterization have several drawbacks when applied to superhydrophobic surfaces. This has resulted in a need to develop new method for characterizing wetting properties of superhydrophobic surfaces.

This thesis presents one auspicious method for wetting characterization of ultra water-repellent surfaces along with the theory the method is based on. In the method a magnetic water droplet is forced to oscillate on the superhydrophobic surface. The friction affecting droplet during oscillations is proportional to the wetting degree of surface. Furthermore, using a moving droplet allows the investigation of dynamic wetting properties of superhydrophobic surfaces.

Avainsanat – Nyckelord – Keywords

Wetting, Superhydrophobicity

Säilytyspaikka – Förvaringställe – Where deposited

Muita tietoja – Övriga uppgifter – Additional information

HELSINGIN YLIOPISTO
HELSINGFORS UNIVERSITET
UNIVERSITY OF HELSINKI

MATEMAATTIS-LUONNONTIETEELLINEN TIEDEKUNTA
MATEMATISK-NATURVETENSKAPLIGA FAKULTETEN
FACULTY OF SCIENCE

Tiedekunta – Fakultet – Faculty	Koulutusohjelma – Utbildningsprogram – Degree programme
Matemaattis-luonnontieteellinen	Fysikaalisten tieteiden koulutusohjelma

Tekijä – Författare – Author

Anna Liski

Työn nimi – Arbetets titel – Title

Wetting Characterization by Driven Ferrofluid Droplet Oscillations

Työn laji – Arbetets art – Level	Aika – Datum – Month and year	Sivumäärä – Sidoantal – Number of pages
Pro gradu -tutkielma	Maaliskuu 2018	57

Tiivistelmä – Referat – Abstract

Superhydrofobisuus tarkoittaa äärimmäistä vedenhylkivyyttä. Ilmiön tutkimus on moninkertaistunut viime vuosien aikana, heti sen jälkeen kun kehittyi keinoja valmistaa äärimmäisen vettähylkiviä pintoja keinotekoisesti laboratorio-olosuhteissa. Superhydrofobisilla pinnoilla on useita lupaavia käyttökohteita korroosion, huurtumisen ja likaantumisen estämisessä. Jotta vettä hylkiviä pintoja olisi mahdollista käyttää sovelluksissa, on tärkeää että niiden kastumisominaisuudet voidaan karakterisoida mahdollisimman tarkasti. Tavanomaiset menetelmät kastumisen asteen määrittämiseen eivät kuitenkaan sovellu riittävän hyvin superhydrofobisuuden mittaamiseen. On tarve uusille menetelmille jotka ovat suunnattu juuri äärimmäisen vettähylkivien pintojen ominaisuuksille.

Tämä tutkielma esittää yhden lupaavan menetelmän superhydrofobisen kastumisen mittaamiseen. Menetelmä perustuu magneettisen pisaran oskillointiin pinnan päällä. Analysoimalla pisaran liikettä on mahdollista selvittää pinnasta aiheutuva kitkavoima joka hidastaa pisaran liikettä. Kitkavoima on verrannollinen kastumisen asteeseen. Menetelmä mahdollistaa kastumisen tutkimisen liikkeen aikana ja tarjoaa tämän vuoksi hyvät lähtökohdat ilmiön mallintamiseen käytännön olosuhteissa.

Avainsanat – Nyckelord – Keywords

Kastuminen, Superhydrofobisuus

Säilytyspaikka – Förvaringställe – Where deposited

Muita tietoja – Övriga uppgifter – Additional information

Contents

Introduction **1**

1 Wetting **4**
1.1 Contact angles 4
1.1.1 Surface tension 4
1.1.2 Shape of drops 5
1.1.3 Young equation 7
1.1.4 Contact angles of real surfaces 9
1.2 Wetting regimes 10
1.2.1 Wenzel state 11
1.2.2 Cassie-Baxter state 12
1.3 Superhydrophobic surfaces 13
1.3.1 In nature 14
1.3.2 Artificial 15

2 Methods for wetting characterization **17**
2.1 Sessile drop method 17
2.2 Tilted plane method 18
2.3 Wilhelmy balance method 19

3 New methods for wetting characterization: ferrofluid oscillator **21**
3.1 Free-decay ferrofluid oscillator 22
3.2 Driven ferrofluid oscillator 23

4 Magnetic materials **24**
4.1 Origins of magnetism 24
4.2 Magnetic ordering 25
4.3 Ferromagnetic hysteresis 26
4.4 Ferromagnetic nanoparticles 27
4.5 Ferrofluids 28

5 Dynamics of oscillations **29**
5.1 Potential energy 29
5.2 Normal force 30
5.3 Horizontal force 30
5.4 Energy dissipation 31

6 Materials and methods **32**
6.1 Project plan 32
6.2 The setup 33
6.3 Magnets 33
6.4 Ferrofluid 34
6.4.1 Ferrofluid properties compared to water 35
6.4.2 Magnetic properties 35
6.5 Surfaces 37
6.5.1 Fluorinated copper surface 37
6.5.2 Nanofilament surface 38
6.6 Data-analysis 39

7 Results and discussion **41**
7.1 Choosing a magnet 41
7.2 Concentration of the ferrofluid 43
7.3 Separation of magnets 44
7.4 Volume of droplet 45
7.4.1 Circular droplet movement 47
7.5 Driving amplitude and driving frequency 49
7.6 Measurements on nanofilament surfaces 49
7.7 Compatibility of simulations with measurements 51

Conclusions **52**

Bibliography **54**

Introduction

Many of us are familiar with the common phrase ”like water off a duck’s back”. It is used when describing something unstickable either physically or metaphorically. The phrase originates from the water-repellent tendency of ducks feathers. Ancient Greeks called this tendency *hydrophobicity* as in ”fear of water”. In contrast to *hydrophilic* materials - materials attracted to water -, hydrophobic materials repel it making them difficult to wet. The wettability of a surface is described by the amount of contact occurring when a droplet of water is placed on top of it. If the surface is hydrophilic the area of contact with the droplet is larger than it would be for a same sized droplet on a hydrophobic surface. Hence the angle of contact the droplet makes with surface is also different. The *contact angle* is a widely used physical quantity for characterizing wetting properties of surfaces, since it is fairly simple to measure and is not affected by the size of droplet as long as the droplet is macroscopic [1]. The surface is considered hydrophobic if its contact angle with water exceeds 90° and hydrophilic if the angle is smaller than that [2].

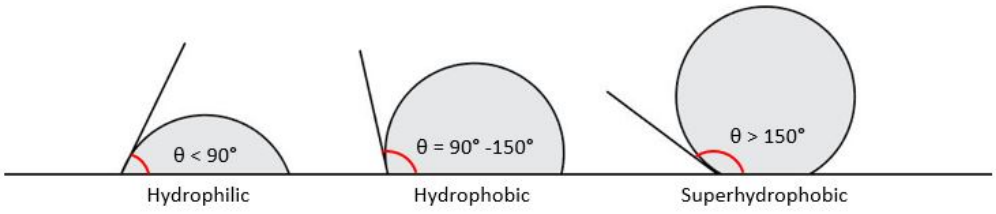

Figure 1: Shape of water droplets on a) hydrophilic, b) hydrophobic and c) superhydrophobic surfaces.

Superhydrophobicity is an extreme form of hydrophobicity. Water-repellency of such surface is so high that droplets on it adopt a round shape. Contact angles on superhydrophobic surfaces are larger or equal to 150° and the roll-off angle i.e the inclination angle of surface at which the drop starts moving is extremely small [3]. In nature many applications of the extreme water-repellency can be found both in plants and animals [3]. Besides the feathers of a duck, some fire-ant species in the

rainforests of Brazil utilize superhydrophobicity of their bodies to survive floods by assembling into floating rafts [4]. Perhaps the most famous example of super water-repellency is the lotus leaf. Due to the low roll-off angle a water droplets on the leafs surface remain highly mobile. Any loose dirt the droplet encounters while sliding along the leaf is attached to it and removed from the surface as the droplet rolls off the edge [2]. The process is known as the *lotus effect* and it enables the plant to keep its leafs permanently clean. It is obvious how this kind of self-cleaning ability applied to other materials would have plenty of potential applications in the fields of technology, construction and textile industry [5]. As a side effect such surfaces also exhibit anti-bacterial properties by preventing attachment of bacteria [6]. Besides the self-cleaning, superhydrophobicity can be applied to reduce unwanted wetting of surfaces in many areas of technology [7]. Other possible applications for water-repellency include drag reduction [9] , corrosion and stain resistance [10], anti-fogging and anti-fouling [5] [11] .

Figure 2: Superhydrophobicity of birds feathers enables them to float on water. Photo by pixel2013/CC0 Creative Commons.

The interest in wetting-resistant surfaces has exploded over the recent years when a group at Kao corporation first introduced a method for preparing superhydrophobic surfaces artificially in the mid '90s [7] [8]. In the following 20 years plenty of methods for the surface preparation have been developed, ranging from as simple as covering a glass surface in soot by burning a match beneath it, to more sophisticated methods [2] [7] [12].

Because of the rapid development in the field of superhydrophobicity it is important to have means for a reliable characterization of surfaces in terms of their wetting properties. The conventional methods for characterization are developed for the most common forms of wetting: hydrophilicity and hydrophobicity. Measuring large contact angles of superhydrophobic surfaces can be problematic due to the pile up of uncertainty factors leading to significant errors in contact angles [13]. This results in a need for a new method for wetting characterization

designed especially for superhydrophobic surfaces. The purpose of the project presented in this thesis is to further the development of one auspicious method for investigating wetting properties of the super water-repellent surfaces.

The method is based on examining the dynamics of droplet movement on the superhydrophobic surface. The degree of droplet mobility on a surface is proportional to the amount of hydrophobicity it exhibits. The method is developed in 2012 at the Aalto University Department of Applied Physics by Jaakko Timonen, Mika Latikka, Robin Ras and Olli Ikkala. In an article 'Free-decay and resonant methods for investigating the fundamental limit of superhydrophobicity' [14], published in Nature Communications a year later, inventors present two methods for characterization of surface wettability.

The work done in this thesis is focusing on finding the optimal measurement conditions and the limitations of the method. The thesis will also serve as the documentation of obtained results. The first chapter is a brief introduction to the theory of wetting and superhydrophobicity. In the second chapter most common methods that are currently used for wetting characterization of the superhydrophobic surfaces are introduced. Third chapter provides an insight to the background research done on the method. Fourth and fifth chapters explain the theoretical framework of the oscillatory method. The sixth chapter is a detailed explanation of materials and methods used in experiments and the seventh chapter is about results.

Chapter 1

Wetting

1.1 Contact angles

The wetting tendency of surfaces is described by contact angles. The contact angle is an angle of contact between solid and liquid measured from the liquids side. On ideally hydrophilic surface, it is favorable for the water to spread as far as possible. The boundary condition of hydrophilicity is reached when the water forms a mono-layer on the surface and the corresponding contact angle is 0° [2]. When for ideally hydrophobic surfaces the contact between surface and the water droplet is unfavorable, corresponding to the 180° contact angle [2]. The contact angles measured are between these two boundary values, since in reality all surfaces are only partially wetting [2]. The surface is considered as hydrophilic if the contact angle of water on it is less than 90° and hydrophobic if it is greater 90° [2]. For superhydrophobic surfaces the contact angle exceeds 150 ° and the roll-off angle i.e. the angle of surface tilt at which droplet begins to move, is less than 5 ° [15]. The wetting characteristics of surface are closely linked with the interactive forces at the interface of water and solid.

1.1.1 Surface tension

Thomas Young was the first person to introduce the idea of *surface tension* in 1805. He noticed that particles within fluid exerted pressure on its surface leading to convex curvature [16]. Modern approach to surface tension has not stemmed far from the original idea. Consider the droplet of homogeneous fluid on a solid surface in gaseous medium. The molecules inside the bulk have neighboring molecules in all directions. The interactive forces between the molecules cancel

each other out either partially or completely resulting in *cohesion* within the fluid. The molecules on the surface interact with the molecules alike from one side and the different molecules of surrounding substance from the other side. The interaction forces between surface molecules and the surrounding substance is referred to as *adhesion*. When the cohesion is stronger than adhesion the most thermodynamically favorable state for the droplet is to minimize it's interfacial area with the surface by taking a rounder shape. If the adhesion is stronger than cohesion, the droplet tends to maximize the area by spreading on a surface. Surface tension is a difference between the cohesional and adhesional forces on the interface and it depends on characteristics of both components of the interface [2]. In addition a droplet resting on a solid surface has a *line tension*, which is a one dimensional case of surface tension at the three-phase line where the solid, gas and liquid phases meet [17].

Considering further the drop of fluid on a solid surface in a gaseous medium. The system has three interfaces: liquid-solid, liquid-gas and the former solid-gas interface which has been replaced by adhesion of the drop [18]. Because of the surface tension, excess energy is needed for breaking the bonds between molecules when creating a new surface [19]. The energy needed is equal to surface tension multiplied by the area of surface created [19]. Likewise the energy is released when the surface is abolished. Provided that the droplet is large enough so that the effects of line tension can be neglected [20], the Gibbs free energy of the system written as

$$G = A_{lg}\gamma_{lg} + A_{ls}\gamma_{ls} - A_{sg}\gamma_{sg} \tag{1.1}$$

where A is the area of the given interface, and γ is the surface tension. The equation describes the energy change in the system when droplet is spreading. Most thermodynamically favorable state for the fluid is when the Gibbs free energy is minimized [18]

$$dG = dA_{lg}\gamma_{lg} + dA_{ls}\gamma_{ls} - dA_{sg}\gamma_{sg} = 0 \tag{1.2}$$

1.1.2 Shape of drops

Upon discovering the surface tension Young also observed the effect it has on the droplet shape resting on a solid surface [16]. By analyzing the near-boundary

contact of the droplet and solid he and derived an expression for the angle of contact. Young stated that slight variation of angle reflects on the variation of interfacial forces by following equation:

$$F_{lg} = F_{sl}cos\theta \tag{1.3}$$

where θ is the contact angle, F_{lg} is interfacial force between liquid and gas F_{sl} is the one of solid and liquid [16]. The force surface exerts on the line of contact is proportional to the small area of the interface close to contact line [21]. The equation 1.3 can be then expressed in terms of infinitesimally small surface areas near contact line [21].

$$dA_{lg} = dA_{sl}cos\theta \tag{1.4}$$

The relation allows to find the variation of Gibbs free energy from the equation 1.2 reaching a Young equation:

$$\gamma_{sg} = \gamma_{sl} + \gamma_{lg}cos\theta_Y \tag{1.5}$$

This simple deviation of Young's equation has later been invalidated since it neglects the impact of contact angle on the whole surface area of droplet. Thus breaking the conservation of volume in a droplet [21]. Despite errors in the original derivation the Young equation has later been validated by derivation with thermodynamic approach that is shown in the next chapter [22].

Young equation shows that the contact angle depends only on surface tensions between phases. However, it is contrary to usual observations where the shape of drop is also influenced by its size [20]. Consider a droplet suspended in air. On the liquid gas interface the surface tension causes droplet to minimize its surface area by taking a shape of a sphere. The energy required for creation of surface is described by the surface tension and area, scaling as γr for the spherical droplet with the radius r [2]. The gravitational forces for the droplet are more heavily influenced by the droplet size, scaling as $\rho g r^3$, with g being the gravitational acceleration constant and ρ density of the fluid [2]. The surface tension becomes dominant force when radius of droplet is smaller below capillary length κ, allowing the gravitational forces to be neglected [20]

$$\kappa^{-1} = \sqrt{\frac{\gamma}{\rho g}} \tag{1.6}$$

Capillary length is important factor to consider when calculating the shape of liquid-gas interface. The shape of droplet is determined by Young-Laplace equation. It relates the radii of curvature R_1 and R_2 to the pressure difference across the surface ΔP [23]. The difference in pressure is caused by surface tension γ_{lg} between liquid and gas phase. For the droplets smaller than the capillary length the Young-Laplace equation can be applied without its gravitational term $(-\rho gh)$ [23].

$$P_{in} - P_{out} = \Delta P = \gamma_{lg}\Big(\frac{1}{R_1} + \frac{1}{R_2}\Big) \tag{1.7}$$

where P_{in} is the pressure exerted on the surface by the liquid phase and P_{out} is the pressure exerted by the gas phase.

1.1.3 Young equation

For a droplet on a flat solid surface, the relation between interfacial tension and the contact angle is described by the Young equation (1.5) [16]. With existing methods, measurable parameters of the equation are contact angle θ and surface tension of liquid-gas interface. The surface tensions where the other component is solid are more problematic to measure since most of existing methods are based on deformation of the surface [24]. Yet the solid-liquid surface tension is the main component indicating wettability of surface. Young equation provides a simple tool in assessing solid-liquid surface tension with easily measurable quantities [24].

Approaching wetting as a thermodynamic phenomenon, Kwangseok Seo et al. presents a method for re-derivation of Young equation 1.5 [22]. Consider a macroscopic droplet with radius smaller than capillary length. Due to negligible gravitational forces it will adapt the shape of spherical cap when resting on flat solid surface [22]. The area of liquid-gas interface, A_{lg}, is then:

$$A_{lg} = 2\pi Rh = 2\pi R^2(1 - cos\theta) \tag{1.8}$$

where R is the radius of curvature and θ the angle between center and the edge of cap as shown in figure 3. The area of liquid-solid and the replaced solid-gas contact is a projection of a drop in vertical plane

$$A_{ls} = A_{sg} = \pi R^2 sin^2\theta \tag{1.9}$$

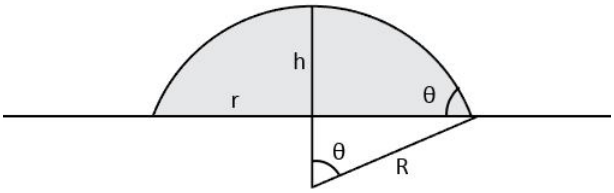

Figure 3: The shape of a small droplet on solid surface is a spherical cap [22].

The equations 1.8 and 1.9 combined with the equation 1.1 yield the following equation for free energy:

$$G = 2\pi R^2(1 - cos\theta)\gamma_{lg} + \pi R^2 sin^2(\gamma_{ls} - \gamma_{sg}) \tag{1.10}$$

At the point of equilibrium the variation of energy is $dG = 0$

$$2\pi R\Big[\gamma_{lg}\Big(2(1 - cos\theta) + Rsin\theta\frac{d\theta}{dR}\Big) + (\gamma_{sl} - \gamma_{sg})(sin^2\theta + Rsin\theta cos\theta\frac{d\theta}{dR})\Big] = 0 \tag{1.11}$$

where the $\frac{d\theta}{dR}$ is found by the condition of retaining the constant volume V of the droplet.

$$V = \frac{\pi R^3}{3}(1 - cos\theta)^2(2 + cos\theta) \tag{1.12}$$

$$\frac{d\theta}{dR} = -\frac{(1 - cos\theta)(2 + cos\theta)}{Rsin\theta(1 + cos\theta)} \tag{1.13}$$

Combining the equations 1.11 and 1.13 and simplifying vigorously leads to Young equation [22]:

$$\gamma_{sg} = \gamma_{sl} + \gamma_{lg}cos\theta_Y \tag{1.14}$$

For ideally flat and homogeneous surfaces the lowest possible value for contact angle is next to 0°. Yet the highest angle is far from the boundary condition of total non-wetting (180°) by being less than 120°in most cases [2]. However, with non-ideal surfaces higher contact angles are observed. This has to do with roughness and heterogeneity of real surfaces.

1.1.4 Contact angles of real surfaces

The local inclinations of a rough surface vary from one point to another. For a droplet on such surface the *actual contact angle* is the angle between liquid and solid on a microscopic scale as is shown in figure 4. The actual contact angle corresponds well with Young contact angle in macroscopic drops when the line tension is insignificant [17]. The problem is that with the current methods only the *apparent contact angle* can be measured, which is the is the angle between the liquid-gas interface and the tangent of solid surface as in the center picture of figure 4 [1]. The difference between actual and apparent contact angle might be significant, and it is crucial to find the relation between them [1].

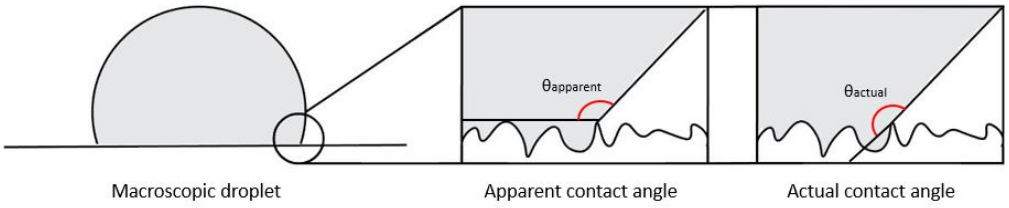

Figure 4: For the droplet on a rough surface actual contact angle may be very different from the apparent contact angle.

On an ideal surface the Gibbs free energy acts as parabola in regards to contact angle with Young contact angle at the energy minimum. Consider a droplet moving slowly on a real surface. Due to the roughness and heterogeneity a contact line in motion encounters multiple barriers like hydrophobic domains and microscopic elevations that restrict the line from advancing [24]. While the hydrophilic domains and declinations of surface do the opposite aiding the advancement of the contact line [24]. This creates local minimums in the Gibbs energy curve which are separated by energy barriers as is shown in figure 5 [1]. Due to local minimums in a Gibbs energy curve the apparent contact angle has a number of stable values. The largest value of the contact angle i.e the angle previous to contact line moving forward, is an *advancing contact angle*. Whereas the *receding contact angle* is the lowest angle before the contact line retreats [1]. The difference between advancing and the receding angle is called a *contact angle hysteresis* and the magnitude of it can be treated as a degree of the surface non-ideality [15].

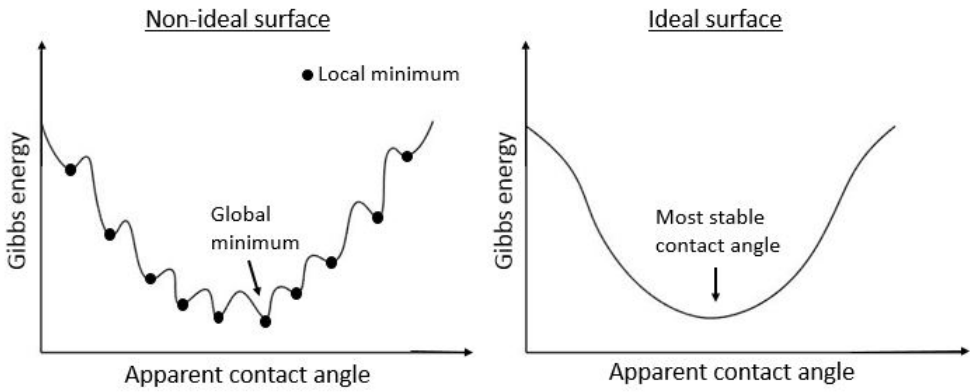

Figure 5: The drafts of Gibbs energy curves on a non-ideal and the ideal surface. The curve of a non-ideal surface has a number of global stable contact angle values for the apparent contact angle due to roughness and heterogeneity of surface.

The contact angle that corresponds to the global minimum of Gibbs energy curve, the *most stable contact angle* is the best approximation of Young contact angle for non-ideal surface [24]. The precise evaluation of the most stable contact angle has been problematic. Most methods for estimating it are performed indirectly by measuring the advancing and receding angle and calculating the average from either angles or their cosines [1]. It is unknown which approach results to a closer approximation of the Young contact angle. [15] It has also been disputed whether the advancing and receding angles can be correlated with the Young's angle at all [15]. The other approach has been taken by T. S. Meiron et. al who evaluated most stable CA directly from the stationary droplet [25]. By predisposing the droplet to vibrations the external energy allows contact line to slip over the energy barriers into global energy minimum. The method has lead to promising results but it suffers from inability to differentiate between the most stable contact angle and the meta-stable states in the proximity since the energy barriers tend to grow when approaching the global minimum [1] [25].

1.2 Wetting regimes

Young's contact angle θ_Y is also referred as an ideal contact angle since the equation is based on the assumption of an ideal solid surface i.e. perfectly smooth, rigid, insoluble, non-reactive and chemically homogeneous [1]. This is rarely the case with real surfaces which have more or less surface structure and possibly heterogeneous composition. The contact angles on a real surface can be very

different than the ideal contact angle. For applications of Young's equation to the real surfaces it is essential to find the relation between ideal and the observed contact angle [1]. An effort has been made to bridge the gap between theory and practice by closer studies of how surface non-idealities impact the ideal contact angle [26] [27].

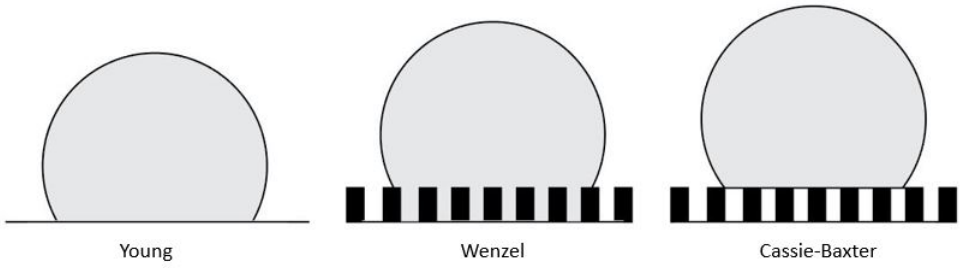

Figure 6: Wetting of ideal surface compared to wetting regimes on rough surfaces.

Two main wetting states are distinguished on a rough surface. The *Wenzel state* is the regime of homogeneous wetting where the liquid penetrates into the roughness of surface. The state is associated with low mobility of droplet, pinning of contact line and large contact angle hysteresis [28]. When roughness of a hydrophobic surface is increased above the critical level, wetting becomes non-homogeneous. A droplet is in *Cassie-Baxter state* when air remains embedded in the cavities of surface structure beneath it. The droplet in this state has low contact angle hysteresis and remains highly mobile. With appropriate surface handling and lubrication, high mobility can also be achieved in Wenzel state [28]. Yet the sliding angle of slippery Wenzel state (18°) remain considerably larger than those of Cassie-Baxter state in superhydrophobic surfaces($< 5°$) [7] [28]. Considering the synthesis of materials with non-wetting properties it is reasonable to pursue Cassie-Baxter state wetting as opposed to Wenzel state slippery or not.

1.2.1 Wenzel state

Robert N. Wenzel identified in his article "Resistance of solid surfaces to wetting by water" that wettability of a surface depends not only on the interfacial tension but on the magnitude of its roughness as well [26]. Just as in the Young model, droplet spreads on a rough surface until it reaches equilibrium characterized by the contact angle. The roughness increases the surface area within unit area, therefore increasing also the intensity of surface energy [26]:

$$G = A_{lg}\gamma_{lg} + KA_{ls}(\gamma_{sl} - \gamma_{sg}) \tag{1.15}$$

Where K is the roughness factor describing the increase in surface energy from the ideal surface. Combined with the equations 1.8 and 1.9

$$G = 2\pi R^2\gamma_{lg}(1 - cos\theta) + K\pi R^2 sin\theta^2(\gamma_{sl} - \gamma_{sg}) \tag{1.16}$$

and the variation of free energy at the point of equilibrium

$$\gamma_{lg}(2(1 - cos\theta) + Rsin\theta\frac{d\theta}{dR}) + Ksin\theta(\gamma_{sl} - \gamma_{sg})(sin\theta - Rcos\theta\frac{d\theta}{dR}) = 0 \tag{1.17}$$

combining the former equation with the equation 1.13 drawn from condition of constant volume, with rearrangement and trigonometric identities yields a familiar looking equation

$$\gamma_{lg}cos\theta = K(\gamma_{sg} - \gamma_{sl}) \tag{1.18}$$

combining further with Young's equation 1.14 a Wenzel equation is obtained [22].

$$Kcos\theta_Y = cos\theta \tag{1.19}$$

Roughness in the surface enhances the wetting characteristics of a smooth surface. The contact angles on the hydrophobic surfaces increase with roughness, while opposite is true for the hydrophilic surfaces [26]. Similar results has been found in the Kao experiment where S. Shibuichi et. al. compared apparent contact angles on the smooth and rough surfaces of same material [8]. The experiment showed that when the roughness of hydrophobic material is increased above the critical value the surface becomes superhydrophobic [8]. The wetting then becomes heterogeneous since the air remains trapped in the roughness of surface.

1.2.2 Cassie-Baxter state

The increase in roughness of the surface above the critical level leads to liquid being unable to slip into the cavities of roughness. Air remains embedded in the cavities leaving the liquid in contact with just the fraction of the solid surface [29]. The wetting regime in called Cassie-Baxter regime and it is the regime of superhydrophobic wetting. Because of air trapping the surface can be considered

as a chemically heterogeneous [27] [29]. Cassie and Baxter derived an equation for this type of wetting which applies also to other heterogeneous surfaces [29].

[22] In the Cassie state the total energy of a system can be written as:

$$G = f_1 A_{sl}(\gamma_{sl,f_1} - \gamma_{sq,f_1}) + f_2 A_{sl}(\gamma_{sl,f_2} - \gamma_{sq,f_2}) - A_{lg}\gamma_{lg} \tag{1.20}$$

Where f_1 is the fraction of one region of a surface and the f_2 is the fraction of second region of surface [22]. The equation can also be extended to multiple fraction areas with the sum of fractions being $\Sigma f_i = 1$. Combining the equation with equations 1.8 and 1.9 the variation of energy at equilibrium becomes

$$(f_1+f_2)(\gamma_{sl}-\gamma_{sg})(sin^2\theta + Rsin\theta cos\theta\frac{d\theta}{dR}) + \gamma_{lg}(2(1-cos\theta) + Rsin\theta\frac{d\theta}{dR}) = 0 \tag{1.21}$$

Combining it with equation 1.13 and rearranging and simplifying gives rise to Cassie-Baxter equation

$$cos\theta = f_1 cos\theta_{Y1} + f_2 cos\theta_{Y2} \tag{1.22}$$

Where the θ_{Y1} and θ_{Y2} are the Young contact angles on a area fraction in question and θ is the apparent contact angle [22]. Considering a droplet on a heterogeneous rough surface in Cassie-Baxter wetting state, the heterogeneity of surface is caused by the air trapped in roughness under the droplet. θ_{Y2} is then 180 and the equation 1.22 becomes

$$cos\theta = f_1 cos\theta_{Y1} - f_2 \tag{1.23}$$

The Cassie-Baxter state is often referred to as meta-stable since the droplet can sometimes fall into Wenzel state when subjected to high pressure, temperature or contamination [28]. The transformation from Cassie-Baxter to Wenzel state is irreversible making the Wenzel state more stable state of wetting [28].

1.3 Superhydrophobic surfaces

The definition for superhydrophobic surface is that exhibits contact angles larger than 150° for water combined with low contact angle hysteresis [5]. These properties are only obtainable when the regime is Cassie-Baxter state of wetting.

For the wetting to be in Cassie-Baxter state the free-energy of the surface must be low and the surface must also be rough [5]. These types of surfaces can be found in nature widely but there are also wide range of bio-inspired artificially prepared surfaces [2].

1.3.1 In nature

Most of the research on natural superhydrophobic surfaces has been focused on the surfaces found in plants [3]. Plants tend to have cuticular wax surfaces [3]. Wax is a hydrophobic material that is found either as a film on the surface or as crystals of varying shapes [3]. The latter one is more connected to the superhydrophobicity since all of the known superhydrophobic plants have this type of cuticular wax structure on their surfaces [3]. The wax crystals form a nanoscale roughness on to the leaf. In addition to that, most of the plants possessing superhydrophobic properties have also micro-scaled roughness beneath the wax crystals resulting from shapes of plants surface cells that form microscopic bumps on the surface [3] [12]. Despite most of the plants exhibiting hierarchical structure of roughness, it is not crucial for achieving a high degree on hydrophobicity [12]. The absence of micro-structure can be compensated with a denser coating on wax crystals, yet this reduces the durability of the surface [2] [3] [5]. Plants with this type of structure usually exhibit superhydrophobicity only for limited period of time [3].

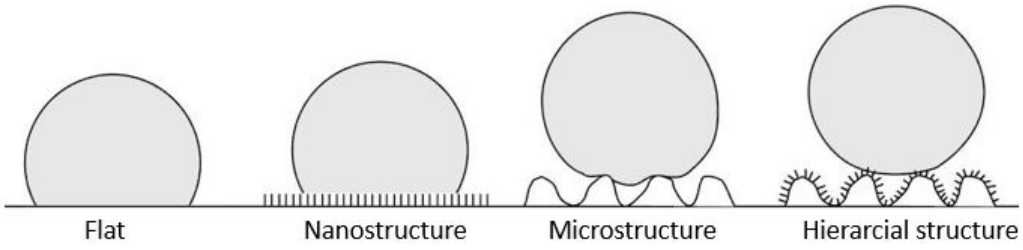

Figure 7: Wetting of different surface structures.

In addition to plants, some insects are also known to have superhydrophobic body parts. Insects achieve superhydrophobicity with slightly different means than plants do [3]. While plants rely on achieving superhydrophobicity through nanoscale roughness of wax crystals, insects rely more on the rough structure of the surface morphology [3]. It is common for flying insects to have superhydrophobic wings since due to small sizes of insects the wetting of wings

might get them to stick together and prove fatal to the creature. Three most common structures found in the insect wings are scales with nanoscale holes in them, fractal structures and tooth-like nanopillars [3]. Some other insects like diving spiders get superhydrophobic with micro-scale hair, setae. By themselves the setaes are not very hydrophobic, but the structure of their surface consist of nanoscale grooves where air is kept embedded during contact with water [3].

Some large animals have superhydrophobic parts as well. Most of birds have water-repellent feathers, like the duck mentioned in the introduction chapter. The superhydrophobicity of the feathers is based on combination of multiscale roughness and water repellent preening oil [30]. The hydrophobicity is thus achieved much with a similar manner as the plants do.

1.3.2 Artificial

Artificial superhydrophobic surfaces mimic the structure of those found in nature. The base principle behind all superhydrophobic surfaces is that the surface material is hydrophobic and its roughness scale is less than the capillary length of water [2]. This leaves huge amount of possibilities in terms of surface geometry and the chemical structure [2]. By choosing the preparation method carefully some specific additional properties can be obtained as well. For example droplet mobility can be improved by decreasing the fraction of solid surface in touch with the droplet or the surface can be made more durable against mechanic stress by using holes instead of pillars in the surface structure and avoiding tall and sharp structures [38]. Higher contact angles can be obtained by using multiple roughness scales, but using single roughness scale with length below the wavelength of visible light provides more transparency to the surface [2]. Different properties along with hydrophobicity can also be achieved by a variety of superhydrophobic coatings.

The wide range of preparation methods results in a variety of surface geometries from random roughness to ordered and textured surfaces like micropillars [12]. For example roughness can be created with nanoscale fibers made with electrospinning, self-assembly of colloidal particles, growing nanocrystals, etching or copying surfaces with templates [2]. The methods can also be combined to create a multiscaled roughness. Lithography is also a commonly used method for producing superhydrophobic surfaces with the advantage of it being production of well-defined surfaces and its good repeatability [2].

In the exparimental part of this thesis are two detailed examples of preparation of artificial superhydrophobic surfaces. One of the methods is based on self-assembly

of hydrophobic fluorothiol onto the sample surface. Superhydrophobicity is achieved by roughening the surface before self-assembly. The other method described is based on growth of nanosize silicone filaments on the surface. The filament structure creates nanoscale roughness on the surface. Silicone is a hydrophobic material and combined with roughness of the surface a very high water-repellency can be achieved.

Chapter 2

Methods for wetting characterization

The methods that are most commonly in use for wetting characterization of superhydrophobic surfaces can be divided into two main categories: direct measurements with contact angle goniometer and the methods based on immersion of the surface in water. While these methods are precise within the hydrophobic-hydrophilic range, extreme contact angles of superhydrophobic surfaces reduce the accuracy of conventional methods.

2.1 Sessile drop method

The sessile drop method is the most commonly used method for evaluating wetting of material [24]. The device contains a horizontal stage on which the surface sample is placed. Above the sample is a micrometer sized pipette that is used to dispense a droplet on the sample surface. Droplet is lit from one side and filmed from the opposite with the enlarging camera. Advancing and receding contact angles are measured separately. In the beginning of the measurement a small droplet is pipetted on the sample surface. During the measurement of advancing contact angle the size of droplet is slowly increased with the needle staying inside the droplet to avoid unnecessary vibrations. When the volume of the droplet increases above the critical size the contact line takes a step forward. The maximum angle of contact before the step is the advancing contact angle. Measuring of the receding contact angle is done by slowly reducing the size of the droplet, receding contact angle being the angle before contact line tacking a step back. In practice the advancing contact angle tends to be smaller and receding contact angle larger than purely theoretical values because of inevitable presence of external energy during measurement [1]. In both measurements the angle is measured by fitting the Young-Laplace equation onto the projection if the droplet

cap. The contact angles are evaluated at the point of intersection of Young-Laplace fitting with the sample surface.

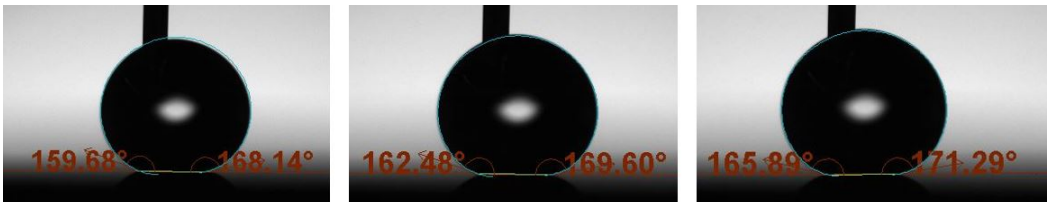

Figure 8: Sessile drop method with 3 different baselines. Choosing a contact point between the droplet and sample is done by operator creating uncertainties in the results.

The benefit of the method is that it needs only a small amount of liquid and just a few mm^2 of the sample surface [24]. On a flip-side contamination of small area on the surface easily distorts the results [24]. Other issues associated with the method is the unsymmetricity of the droplet leading in different contact angles from different sides [24]. Also with the measurements done on the small area of surface the method can not be easily applied to the larger surface areas. With superhydrophobic surfaces additional issue is the distortion of the droplet bottom due to gravity [13]. Method is also dependable on the operator choosing the position of the baseline of droplet-surface contact [24]. Combined with other uncertainties of the measurement this leads to somewhat arbitrary results when measuring superhydrophobic surfaces.

2.2 Tilted plane method

Tilted plane method is a modification of the sessile drop method [24]. After pipetting the droplet on the sample the needle is removed from inside of the droplet. Measurement is done by tilting the sample plane until the droplet rolls of the sample surface. The advancing and receding contact angles are obtained simultaneously at the moment before the droplet rolls of the surface [24]. The contact angle at the highest point of droplet is considered to be the receding contact angle, and the contact angle at the lowest point of droplet is the advancing contact angle. The accuracy of method depends on the surface wetting properties [31]. For hydrophilic surfaces the largest contact angle at the bottom of a droplet is equivalent to the advancing contact angle, while the smallest contact angle on the droplets top can be much higher than the value of the receding contact angle [31]. For the hydrophobic surface the situation is exactly the opposite, the receding contact angle equals to the smallest contact angle on the top

of drop while the maximum contact angle can be smaller than the advancing contact angle [31]. As a consequence the hysteresis cannot be reliably obtained from the measurements on the inclined plane and the roll off angle can not be calculated from the advancing and receding angles alone [31].

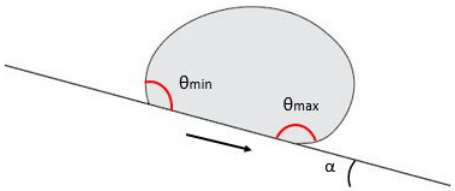

Figure 9: The tilted plane method. Advancing and receding contact angles are not directly comparable with smallest and largest sliding angles.

2.3 Wilhelmy balance method

In wilhelmy balance method the contact angle is obtained indirectly by measuring the force of wetting. Method utilizes a thin smooth vertical plate suspended above the dish of water. Sample is slowly immersed in liquid while its weight is measured at the same time [24]. Due to the force of wetting and the buoyancy the measured weight of the plate changes as the plate continues to be immersed further. The change in weight follows the equation

$$\Delta F = \gamma_{lg} p cos\theta - V \Delta \rho g \tag{2.1}$$

Where the first term is the force of wetting and the latter one is the contribution of buoyancy. In the first part of the equation θ is the contact angle between liquid an solid and the p is the perimeter of the contact line. In the buoyancy describing part of the equation V is the volume of the sample immersed in water $\Delta\rho$ is the density difference between the gas and the liquid phase and g gravitational coefficient [24]. Equation shows that when the sample is hydrophilic ($cos\theta < 0$) the force of wetting is positive and the liquid level rises up until the balance between gravity is reached. On the other hand when the sample surface is hydrophobic ($cos\theta > 0$) the surface resists wetting and the water recedes from the sides of surface [24]. The advancing contact angle is calculated from the wetting force that is measured when the plate is being submerged in water while the receding contact angle is calculated when the plate is lifted up [24].

Benefit of the method is that the plate can be also submerged in water with different speeds allowing the studying of wetting dynamics [24]. On the flip-side for the accurate measurements the cross section of the sample must be the same through out the sample creating some restrictions for the applicability of the method [24]. The result for the contact angle is averaged value and reflects the properties of the whole sample which can be misleading if the sample is very heterogeneous. The smoothness of the wetting force curve reflects the heterogeneity of the sample to some degree but not entirely [24]. Additionally, the method can not be applied to the cases where the area of interest is very small and the measurement itself can affect the results since the sample can swell and absorb some water during the immersion [24].

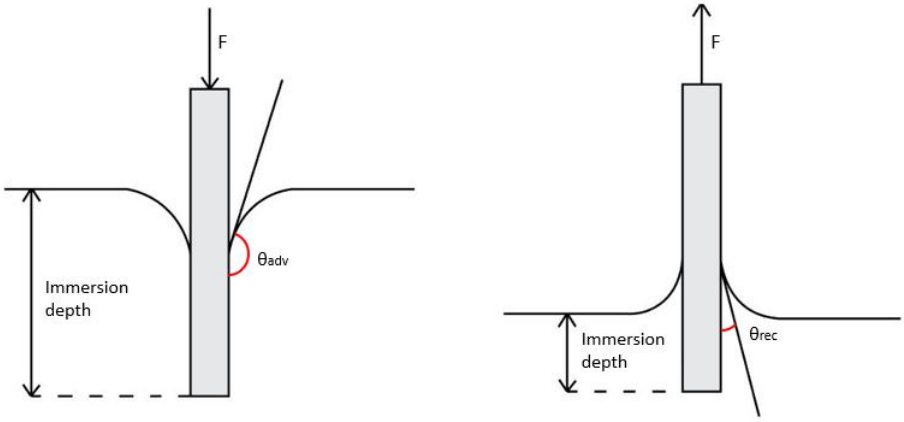

Figure 10: The wilhelmy balance method. Advancing contact angle is measured by submerging the plate in water while receding contact angle is measured by lifting the sample.

Chapter 3

New methods for wetting characterization: ferrofluid oscillator

The field of superhydrophobicity is growing fast and to use such surfaces in applications it is vital to have the ability to characterize wetting properties precisely. Yet the conventional methods have some evident disadvantages in determining the contact angles on highly water-repellent surfaces. Both sessile drop and the plate based methods are in static or close to static conditions [32]. Static conditions are being favored because the process of wetting is delicate and bringing extra energy to the system can lead to distorted results. However, most of the everyday wetting happens in non-static conditions and the wetting process can be different than in static case. New methods for characterization of dynamic wetting properties of surfaces, especially in superhydrophobic range, are needed [33].

Examining the droplet movement on a superhydrophobic surface is a new approach for the characterization of wetting. J. Timonen et. al. have examined the possibilities for characterization by inducing oscillations of a droplet on superhydrophobic surface [14]. The oscillations are dampened by dissipation forces that are related to the surface friction and the viscous dissipation inside the moving droplet. The dissipational forces are very small due to small size of the system and low adhesion of a droplet to the surface. Oscillatory methods are advantageous for investigating small energy dissipations due to their increase in measurement accuracy with the decrease in the measured forces [14].

3.1 Free-decay ferrofluid oscillator

To induce oscillations a small amount of magnetic iron-oxide nanoparticles is dispersed in water. Movement of *ferrofluid* droplet can be controlled by a magnet placed under the surface. For the experiments in [14] the droplet was released onto the surface from the side of the magnet. This created gradually decaying oscillatory motions in the droplet pictured in figure 11.

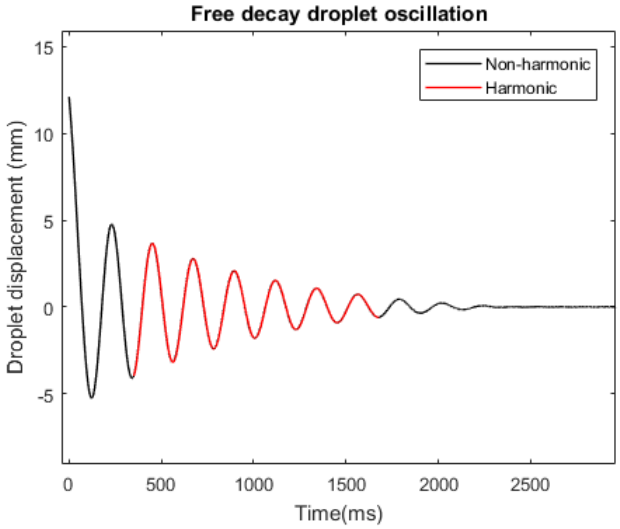

Figure 11: Freely decaying droplet oscillations on a superhydrophobic surface after the release onto the surface. The estimation for the harmonic part of oscillations marked as red.

Fitting equation for dampened harmonic oscillator on the middle part of oscillations makes it possible to obtain the dampening parameters of the droplet movement. The first couple of oscillations are non-harmonic and therefore excluded from the harmonic approximation [14]. Additionally the last few oscillations are also neglected due to increased probability of droplet pinning. From the harmonic fit the dampening parameters, one of which is the coefficient for the surface friction, can be extracted.

The freely decaying oscillatory method has been shown to be highly repeatable and suitable for characterization of non-homogeneities of superhydrophobic surfaces [14]. With the method the surface friction can be extracted with the accuracy close to $10nN$ [14]. However the droplet oscillations dampen far too quickly on the less hydrophobic surfaces for extraction of frictional forces. This limits the applications for the freely decaying method only to the surfaces that are approaching the fundamental limit of superhydrophobicity [14]. By bringing excess

energy to the system throughout the measurement with oscillating the magnet beneath the surface the writers of [14] have developed another variation of oscillatory method. Oscillating the magnet forces droplet to move on the surface and thus enables the characterization of wider range of surfaces.

3.2 Driven ferrofluid oscillator

By driving the droplet oscillations with magnet movement the precision of oscillatory method can be further increased [14]. Movement of magnet beneath the surface forces the droplet to oscillate in time-varying magnetic field and the amplitude of the drop is strongly dependent on the frequency of magnet oscillation. At the frequencies close to droplet resonance frequency the amplitude of droplet was observed to become several times larger than the driving amplitude. The position of the resonance peak on the frequency-scale depends primarily on the iron-oxide concentration and the magnetic field that is affecting the droplet.

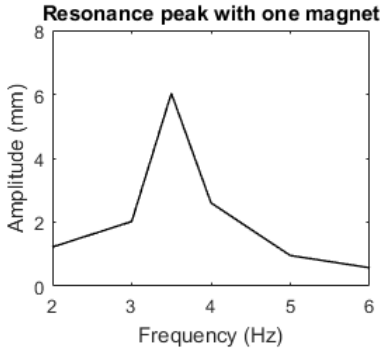

Figure 12: Resonance peak of the ferrofluid droplet. The droplet was oscillated with different frequencies of the driving magnet with an amplitude of 0.5mm.

The writers have compared the resonance peak to the theoretical predictions for the droplet amplitudes and obtained frictional forces of the surface along with the forces associated with viscous dissipation [14]. The driven oscillatory method is promising in terms of its potential applicability to the less hydrophobic surfaces. The results of the method are also shown to be in line with contact angle measurements by sessile drop i.e larger frictional forces were measured on the surfaces with high contact angle hysteresis.

Successful demonstration of functionality of wetting characterization by driven oscillations has given rise to an interest in further investigations. The project done for this thesis is focusing in furthering the preliminary research of J. Timonen et. al. [14] in terms of optimizing the measurement system for as wide as possible surface-applicability.

Chapter 4

Magnetic materials

A magnet is an object that creates a magnetic field. The field is invisible but it generates a pulling or repelling forces in materials that respond easily to the magnetic field and other magnets. The first recordings of magnetism are from ancient Greek when people discovered naturally occurring rocks rich in magnetite - lodestones [34]. For centuries magical properties were associated with these peculiar objects ranging from protection against reptile bites to bringing money and success for their owner [35]. Fast forward to the modern times and the magnetism has been harnessed wildly for the uses of humanity in the modern technology [34]. This is made possible by the increased understanding of magnetic phenomena due to tireless research done in the field.

4.1 Origins of magnetism

In essence the magnetic properties of materials originate from atomic electrons [34]. Every electron in an atom has a total magnetic moment that is result of its intristic spin and orbital movement around the nucleus. The orbital moment can be explained by Bohr atomic model where the electron creates a current loop while circulating the nucleus pictured in figure 13. The angular momentum l of the electron movement is expressed as:

$$l = m_l \hbar \tag{4.1}$$

where $\hbar$ it reduced Planck constant and m_l is an integer value known as orbital magnetic quantum number. The angular momentum is proportional to magnetic moment by

$$\mu = ql/2m_e \tag{4.2}$$

q being elementary charge and m_e mass of the electron. The natural unit for magnetism, Bohrs magneton μ_B, is the result for equation 4.2 when the magnetic quantum number $m_l = 1$. Despite of electrons intrinsic spin being unrelated to orbital movement, magnitude of the spin magnetic moment is also approximately one Bohrs magneton ($1.00116\mu_B$) [34]. Spin of electron has a quantum number of $\pm 1/2$ resulting in magnetic moment having only two possible orientations anti-parallel to each other: 'up' and 'down' [34].

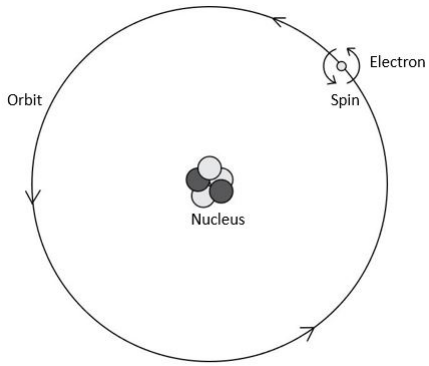

Figure 13: The Bohr atom. Magnetic properties of the material arise from the movements of the charged particle (electron). The nucleus also has a total magnetic moment yet due to large mass of it the moment is a fraction of that of the electrons and can be considered negligible [34].

The total magnetic moment is the result of spin-orbit interaction that follows the laws of quantum mechanics. For our purposes it is sufficient to say that in most atoms these interactions cancel out with an exception of a few transition metals that have non-zero magnetic moments on atomic scale [34].

4.2 Magnetic ordering

In the materials composed of atoms with non-zero total magnetic moments the magnetic properties on macroscopic scale are determined by ordering of atomic moments [36]. In *paramagnetic* materials the ordering is random leading to a zero total magnetic moment in the absent external field. When the magnetic field is applied to paramagnetic material its atomic moments arrange in parallel to the applied field and the matter becomes magnetized. The magnetization leads to the material having positive and negative poles, like a magnet. When the magnetic field is removed the atomic moments become un-arranged once again due to thermal motion and material loses its magnet-like behavior [36].

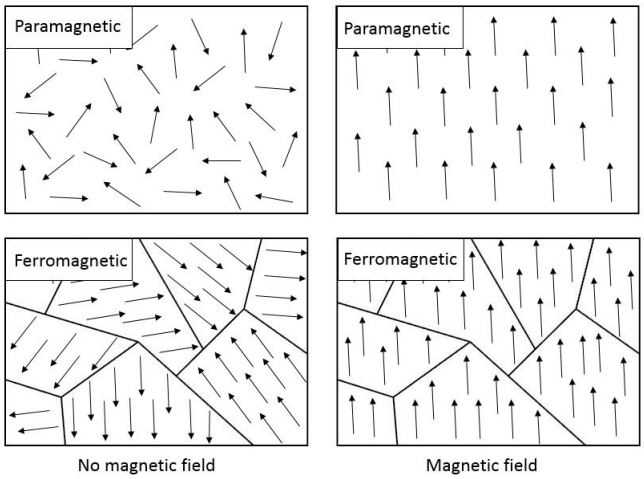

Figure 14: The ordering of magnetic moments in paramagnetic and ferromagnetic materials in the absent and present magnetic field.

In *ferromagnetic* materials the interaction forces between individual magnetic moments overcome the effects of thermal motion [36]. The magnetic moments then tend to arrange in the same direction with those of neighboring atoms forming *magnetic domains*. Inside of one domain all of atomic moments point in the same direction and the domain itself has a net moment. A bulk of ferromagnetic material however, consists of multiple magnetic domains that are in ground state arranged. The magnetic moments of domains therefore cancel out and material appears non-magnetic in the absence of magnetic field. When the field is applied the atomic moments of ferromagnetic material rotate to align with it, much like in the paramagnetic material. The difference between ferromagnetic and paramagnetic behavior is that the presence of domains allows ferromagnetic material to resist disarrangement by thermal motion. Once magnetized ferromagnetic material retains its magnetization even when the external field is removed. Heating a ferromagnetic over its characteristic Curie temperature increases thermal motion over the critical threshold. Atomic moments become decoupled and the material starts exhibit paramagnetic properties.

4.3 Ferromagnetic hysteresis

The response of ferromagnetic material to the external magnetic field has a history dependency known as *hysteresis*. When magnetic field is applied to ferromagnetic material its magnetic domains arrange and the material becomes magnetized. Increasing the field increases the magnetization as well until the saturation point is reached. At saturation point the material exhibits maximum magnetization and cannot be further magnetized by stronger magnetic field. Reducing the field back

to zero leaves part of magnetic domains ordered. The magnetization occurring in a material at this point is known as *remanence*. Together with *coercivity*, the magnitude of applied field in opposite direction for removal of leftover magnetization, remanence describes the 'magnetic hardness' of material. Increasing further the magnetic field in opposite direction past the point of coercivity leads again to saturation magnetization yet this time in the opposite direction as is pictured in the figure 15 [36].

Hard magnetic materials have broad hysteresis loops. Their tendency to remain highly magnetized after removal of external magnetic field makes the well suitable for manufacturing permanent magnets. Soft magnetic materials lose magnetization more easily leading to the more narrow hysteresis loops.

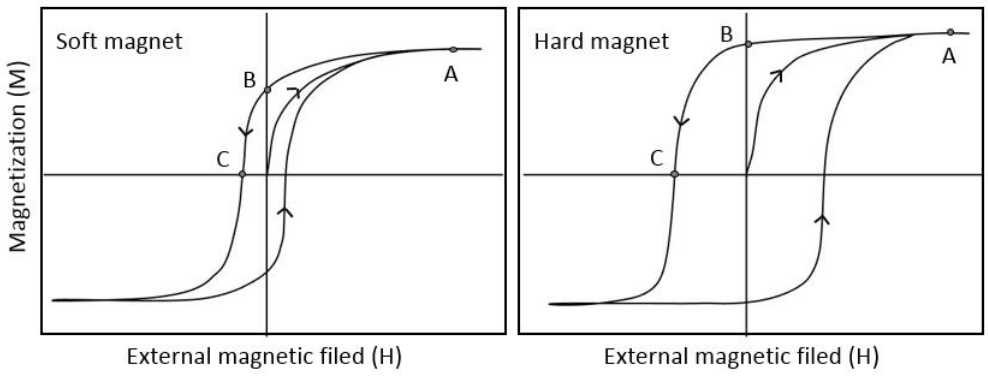

Figure 15: Schematic hysteresis loops of soft and hard magnetic materials. In the pictures A) Saturation point, B) Remanence and C) Coercivity.

4.4 Ferromagnetic nanoparticles

Materials often exhibit different optical, mechanic and magnetic properties as nanoscale objects than in a bulk form [36]. A nanoparticle is defined as a particle that has a size is in nanometre range in all three dimensions. Small nanoparticles have only one magnetic domain meaning that the particle itself has a total magnetic moment.

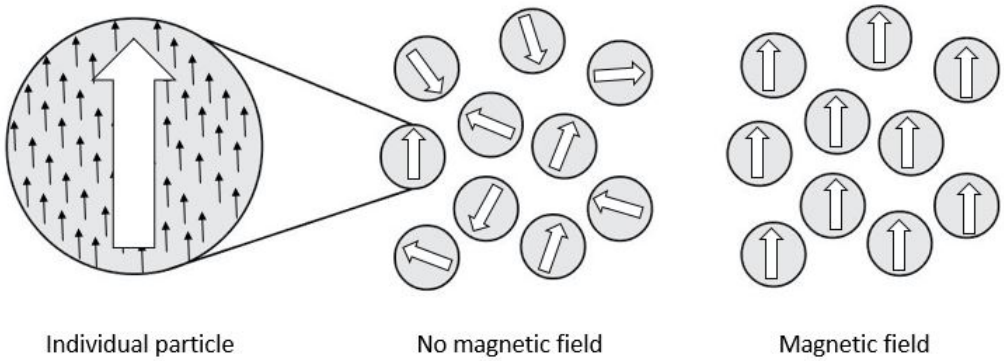

Figure 16: Superparamagnetic nanoparticles are single-domained. In the smallest of particles Brownian motion at room temperature is sufficient for un-arranging the net magnetic moments of particles when the magnetic field is removed.

In the ferromagnetic nanoparticles with smaller diameter than $d \approx 20nm$ the response to external magnetic field begins to resemble that of paramagnetic material and is known as *superparamagnetism*. For small single-domained nanoparticle the thermal energy at room temperature is enough for relaxing the magnetization direction along the 'easy axis' of the particle. The easy axis is the most energetically favorable direction for the alignment of the magnetic moments due to anisotropy of the particle [36]. Coercivity present in the bulk form of same material disappears when the particle size is small enough.

4.5 Ferrofluids

Ferrofluids are magnetic liquids that are formed by suspending superparamagnetic nanoparticles in water or oil medium. The suspended particles allow the manipulation of fluid with external magnetic fields. It is energetically favorable for the small particles to form chains in the external magnetic field due to dipole-dipole interactions [36]. To avoid the chain-formation and other aggregation of tiny particles the fluid needs to be stabilized. Dipole-dipole interactions can be weakened by increasing the distance between particles. This can be achieved by embedding each magnetic particle in polymer or coating it with surfactant [34]. For the water-based ferrofluid surfactant coating is also crucial for preventing the break down of the particle by ionic interactions [34]. The magnetic colloids are further stabilized by Brownian motion preventing sedimentation due to gravity.

Chapter 5

Dynamics of oscillations

The position of ferrofluid droplet resting on a superhydrophobic surface can easily be manipulated with magnetic fields. In the setup used for our experiments a superhydrophobic surface is positioned between two magnets so that the centroid of the ferrofluid droplet is at exact middle point between them. Oscillating the magnets creates a horizontal force in a droplet that points towards the magnet axis causing the droplet to follow magnets. The droplet movement is inhibited by dissipation forces resulting from surface friction and the velocity-related movement of fluid inside the droplet [14].

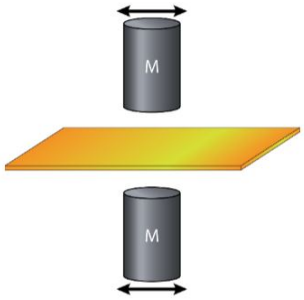

Figure 17: Schematic picture of the setup for the driven ferrofluid oscillator device. The superhydrophobic surface is positioned between two magnets so that the droplet centroid is at the center between the magnets. Picture by Mika Latikka.

5.1 Potential energy

Consider the ferrofluid droplet positioned on a surface in the setup described above. The magnetic potential energy of the drop is minimum on magnet axis. Total potential energy U_{tot} of droplet is a result of magnetic and gravitational fields acting on it [14]

$$U_{tot} = \int_V (-\mu_0 MH + \rho g z) dV \tag{5.1}$$

where μ_0 is the permeability of vacuum, V droplet volume, M magnetization of drop and H the magnetic field within the droplet. The droplets used for our experiments are very small, most common volume being $5\mu l$. It can be therefore approximated that the magnetic and gravitational fields are constant at all points inside the droplet. The total potential energy with this approximation is

$$U_{tot} \approx -\mu MHV + mgz \tag{5.2}$$

5.2 Normal force

The normal force F_N acting on ferrofluid droplet can be extracted by evaluating the total potential energy gradient along the vertical axis

$$F_N = -\frac{dU_{tot}}{dz} = \mu V \frac{dH}{dz}(M + \frac{dM}{dH}H) - mg \tag{5.3}$$

when the droplet centroid is positioned exactly at the center point of the two magnets the gradient of field $\frac{dH}{dz} = 0$. The first term of the equation 5.2 that describes the magnetic vertical force disappears and the normal force equals to the gravitational part only

$$F_N = -mg \tag{5.4}$$

In the two magnet system the vertical forces exerted on the droplet by two magnets cancel out. Since the goal of the experiments is to model wetting by water it is favorable to have gravitational component as the only vertical force.

5.3 Horizontal force

As opposed to the vertical forces, horizontal forces of two magnets do not cancel out. On the horizontal axis parallel to the surface the position dependency of the magnetic field can be approximated as

$$H(x) = H_0 - cx^2/2 \tag{5.5}$$

Where H_0 is the maximum field strength found on the axis of magnets, c is curvature of the field and x is displacement from the axis [14]. The approximation is valid when the displacement from the magnet axis is small [14]. The magnetic

potential energy of the droplet $U_{mag} = -\mu_0 MHV$ is increased when it is displaced from the magnet axis and the restoring force is then

$$F_H(x) = -\frac{dU_{tot}}{dx} \approx -\mu_0 Vc(M + H\frac{dM}{dH})x \tag{5.6}$$

With small displacements the force can be described with the Hookes law $F_H \approx -kx$ where k is constant [14]. The force is always directed to the magnet axis. The oscillations of the magnets add time-dependence to the displacement of droplet from the magnet axis. This translates to horizontal force by

$$F_H(x,t) \approx -k[x - x_{mag}cos(2\pi ft)] \tag{5.7}$$

where the x_{mag} is the magnet amplitude and f frequency of the magnet movement.

5.4 Energy dissipation

The energy dissipation is composed of the frictional dissipation between the droplet and surface along with viscous dissipation caused by fluid inertia. The viscous force is linearly dependent on the drop velocity [14]

$$F_\eta = 2\beta\frac{dx}{dt} \tag{5.8}$$

where β is the viscous dissipation coefficient. The viscous dissipation is proportional to the contact area between the droplet and surface as well as velocity of the droplet [14]. The frictional force between the droplet and surface is not dependent on velocity but is is proportional to the length of contact line by

$$F_\mu = \frac{1}{2}l\gamma_{lg}(cos\theta_{rec} - cos\theta_{adv}) \tag{5.9}$$

where l is length of the contact line, θ_{rec} is the receding contact angle and θ_{adv} the advancing contact angle. The dissipational forces inhibit the motion of droplet along the surface and the force affecting droplet during horizontal movement is

$$F_{tot} = \pm F_H - F\eta \pm F_\mu \tag{5.10}$$

With F_μ always in the opposite of droplet movement.

Chapter 6

Materials and methods

6.1 Project plan

The project done for the thesis is a first sub-part of larger project with an aim to investigate the wetting characterization method more closely. The project is divided roughly into five smaller parts. The first part is the optimization of the method to make it applicable to as wide range of hydrophobic surfaces as possible without compromising the accuracy of measurement. The optimization is done by finding the right combination of parameters in the system. The parameters are pictured in the figure 18.

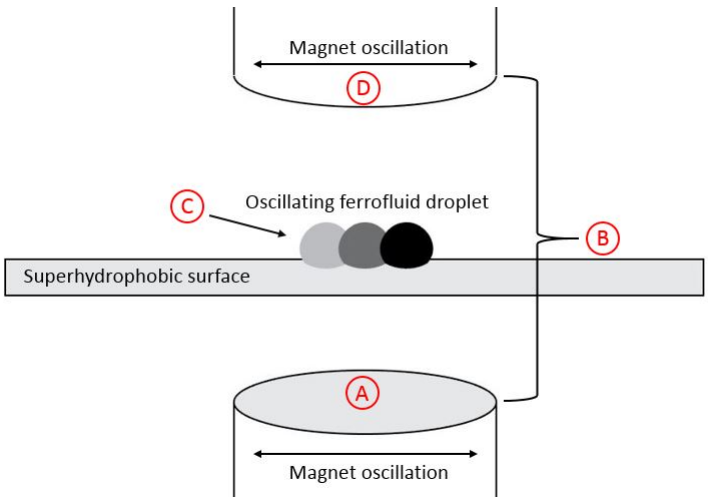

Figure 18: The parameters associated with optimization of driven ferrofluid oscillator. Magnet size (A), separation of two magnets (B), ferrofluid droplet volume and concentration (C) and the frequency and amplitude range of the magnet oscillations (D)

The second sub-part of project is about finding the limitations of the method posed by the range of surfaces that can be investigated and effect of the surface structure on the measurements. Third part is method validation by repeating the measurements and evaluating the applicability of the results to the real-life wetting combined with consideration of possible error sources. Fourth part is to build a functioning prototype and last part of the project is developing an implementing a calibration method to the prototype.

6.2 The setup

The setup used for our experiment is pictured in the figure 19. The setup is attached from the bottom to a motorized linear stage (Aerotech PRO165LM) responsible for horizontal movement of magnets. The stage is controlled by computer along with another motorized stage, a vertical stage (Aerotech MPS50SL) that is used for placing the droplet at the middle point of magnets by controlling the position of the surface.

The magnets are separated by manually adjustable vertical stage that is used for changing the separation of magnets. The two holder cups are attached to the stage each containing three screws used for fixing the magnet inside the cup. During the measurements magnets oscillate simultaneously while a high speed camera (Phantom Miro 310) films the oscillations from the front of the setup.

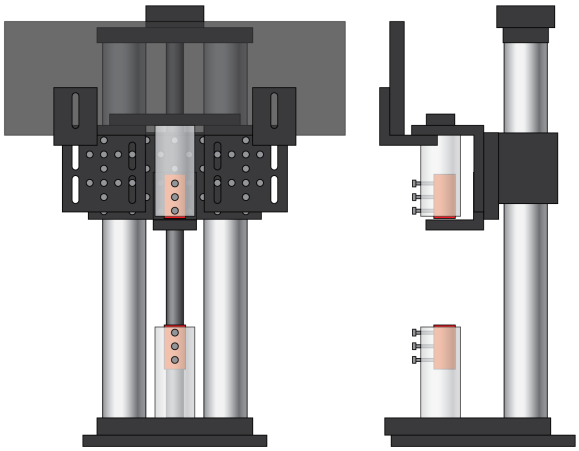

Figure 19: A front and the side view of the setup used for driven oscillator experiments. The magnets are colored red inside the holder cup that is used for fixing them in place. The vertical stage in the picture is used for controlling the separation of magnets. Picture by Mika Latikka.

6.3 Magnets

One of the parameters in the device optimization is choosing the magnet size for the prototype. In the experiments we have used three different magnet sizes for

driving the ferrofluid droplet oscillations. Largest magnets have a diameter of 2.6cm and can narrowly fit in the holder cup. The medium sized magnets have the diameter of 1.9cm and the smallest magnets 1.2cm. All of the magnets are cylinder shaped permanent ferromagnets that are axially magnetized. The material of the magnets is a combination of neodymium and iron with a thin layer($\approx 20\mu m$) of nickel coating on the surface to improve durability of the magnet [37].

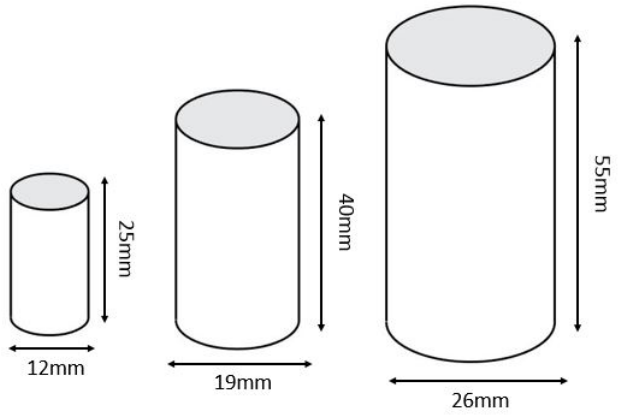

Figure 20: The three magnet sizes used for the experiments. Magnets are cylinder shaped permanent ferromagnets magnetized along the longest axis.

6.4 Ferrofluid

The ferrofluid used for the experiments is synthesized based on the recipe created by J. Timonen. Details of the synthesis are not included in this thesis since the recipe is yet unpublished. Synthesis starts by mixing Iron(II) Chloride Tetrahydrate and Iron(III) Chloride Hexahydrate in a suitable proportions with water. The mixture results in red-orange solution from which the nanoparticles are created by stirring ammonium hydroxide into the mixture. The nanoparticles emerge in the matter of seconds turning the liquid pitch-black. To prevent aggregation the ferrofluid is stabilized with citric acid. The suspension is then washed repeatedly with acetone-water solution to remove impurities and particles that are too small. Ferrofluid concentrate is created by placing a strong magnet under the dish and pouring rest of liquid out from the side. Due to the strong magnetic field small particles cling to the bottom of the dish and form a black blob of ferrofluid. The concentrate is then left to evaporate in ambient conditions until the volume percent of nanoparticles is close to 6%. Formed ferrofluid is water based black solution that has neutral pH with the average size of nanoparticles $r = 4.6 \pm 1.4nm$ [14].

6.4.1 Ferrofluid properties compared to water

For the usage of ferrofluid in wetting characterization it is crucial for it to have similar physical properties as water. Before the experimental use the ferrofluid concentrate is diluted. A dilute solution with $0.2\%_{vol}$ of nanoparticles has the surface tension of $72.5 \pm 0.2 mNm^{-1}$ which is the same as pure water within the error margin $72.6 \pm 0.3 mNm^{-1}$ [14]. The viscosity of fluid is $1.01 \pm 0.02 mPas$ being slightly larger than measured viscosity of water $0.97 \pm 0.02 mPas$ [14]. The increase in viscosity is explained by the Einstein model that predicts the increase in viscosity due to dispersed solid particles by $5\phi/2$ where the ϕ is the volume fraction of particles [14]. For the wetting characterization purposes the difference can be considered small enough to be neglected.

6.4.2 Magnetic properties

Magnetic properties of ferrofluid dilutes of $0.2\%_{vol}$ and $0.15\%_{vol}$ were characterized by VSM-magnetometer (Quantum Design Physical Property Measurement System (PPMS) Dynacool). The fluid is sealed in an air-tight capsule and placed inside the magnetometer. The magnetometer vibrates sample in the altering magnetic field and records the magnetization of it [38]. To examine time induced changes in magnetic properties of ferrofluid, four consecutive characterizations were preformed on the $0.2\%_{vol}$ fluid separated by a month time periods. The results are pictured in the figure 21.

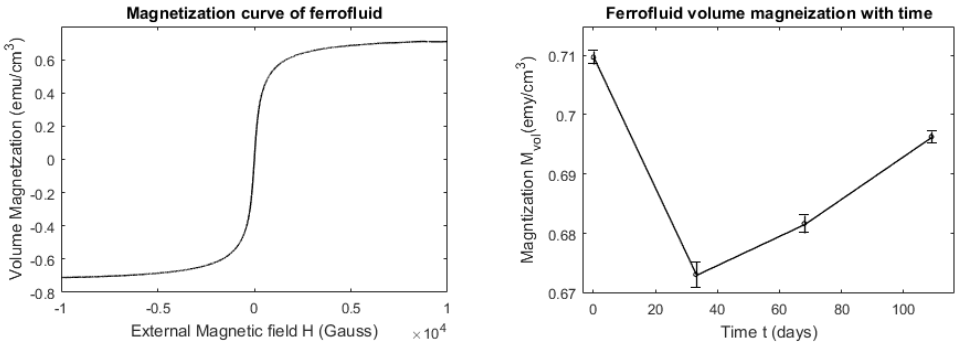

Figure 21: The magnetization curve of the $0.2\%_{vol}$ ferrofluid **(left)**. The saturation magnetization of the $0.2\%_{vol}$ ferrofluid measured in the duration of three months **(right)**.

Saturation magnetization is reduced rapidly during the first month and shows a slight increase during the second and third month. Reason behind the decrease might be explained by the oxidation of nanoparticles. During the experiments the bottle is opened frequently and ferrofluid gets in contact with surrounding air. R. L. Rebodos and P. J. Vikesland have studied the effects of oxidation on magnetization in the water-based ferrofluid [39]. The particle size in their experiments was slightly larger($\approx 10nm$) than in our ferrofluid, yet the particle size might not be relevant for oxidation. If anything, small particles should oxidize more rapidly than the large ones due to larger surface to volume ratio. The oxidation has been found to reduce the saturation magnetization of iron-oxide nanoparticles $5-10\%$ due to changes in crystalline order [39]. The magnetization of our ferrofluid has been reduced by 5% during the first month. The total decrease in our ferrofluids magnetization may actually be larger than measured due timing of the reference magnetization measurement. In the [39] the writers have preformed the first magnetization measurement almost immediately after the fluid preparation. In our case the first magnetization characterization is done couple of days after the synthesis and the fluid might have been partly oxidized. The changed color of ferrofluid in figure 22 supports the assumption of chemical changes in the liquid.

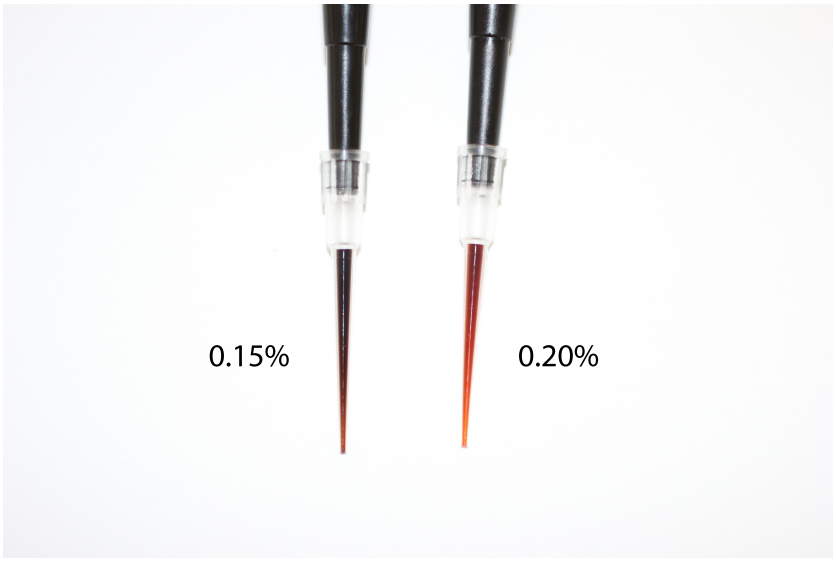

Figure 22: The color difference in $0.15vol-\%$ and $0.2vol-\%$ ferrofluids due to the oxidation of the latter one. The $0.15vol-\%$ ferrofluid on the left was diluted on the day picture was taken. Despite having lower concentration it is noticeably darker than $0.2vol-\%$ ferrofluid diluted two months in prior.

The increase in the magnetization during the rest of the observation period could also be explained by the frequent opening of the ferrofluid bottle. During the three month period the bottle is opened countless of times. Evaporation of water into outside atmosphere during the times bottle is opened could have increased the concentration of nanoparticles inside the bottle. Partly this might also explain the smaller decrease in ferrofluid magnetization during the first month.

Other plausible reason for the gradually increasing magnetization is the aggregation of nanoparticles within the fluid. N. S. Mousavi et al have studied the chain formation of nanoparticles in strong magnetic field [40]. In the study they have found that under suitable conditions ferrofluid nanoparticles form aggregates even in absent magnetic field. Aggregation might cause an increase in the magnetization of the sample since the bulk magnetization per volume is often larger than nanoparticle magnetization per volume [40].

6.5 Surfaces

Two types superhydrophobic surfaces have been used for our experiments. The fluorinated copper surface was used to test the method for a very high contact angle superhydrophobic surfaces. To ensure the applicability of it also on less hydrophobic surfaces the silicone nanofilament surfaces were used.

6.5.1 Fluorinated copper surface

The fluorinated copper surface is used as a highly superhydrophobic surface in our experiments. The average contact angle of the surface is $\theta = 176.5 \pm 2^\circ$ and the hysteresis $\Delta\theta = 5 \pm 1^\circ$ [14]. In addition to being extremely hydrophobic the surface is also very fragile and touching in will result to loss of superhydrophobic properties. Copper surface is so delicate that even repeated oscillations of the ferrofluid droplet will decrease the water repellency of the surface. Due to fragility the surface has to be synthesized frequently and handled with caution while measuring.

Surface is synthesized by following the process described by [33]. The copper plate is polished with sandpaper to remove contamination and to create micro-scale roughness. The plate is then rinsed with acetone and placed in the sonicator for 4 min to remove any loose copper powder from the surface. Silver coating is added on the surface by immersing the plate in the $AgNO_3$-water solution for exactly 1

min. Plate is then rinsed with de-ionized water and dried under nitrogen flow. A fluorothiol coating is added on top of silver by immersing the copper plate in 3,3,4,4,5,5,6,6,7,7,8,8,9,9,10,10,10-heptadecafluoro-1-decanethiol (HDFT) solution in dichloromethane for 10min. Plate is then immersed twice in dichloromethane for removal of excess HDFT not attached to silver coating and left for a moment under ambient conditions to evaporate.

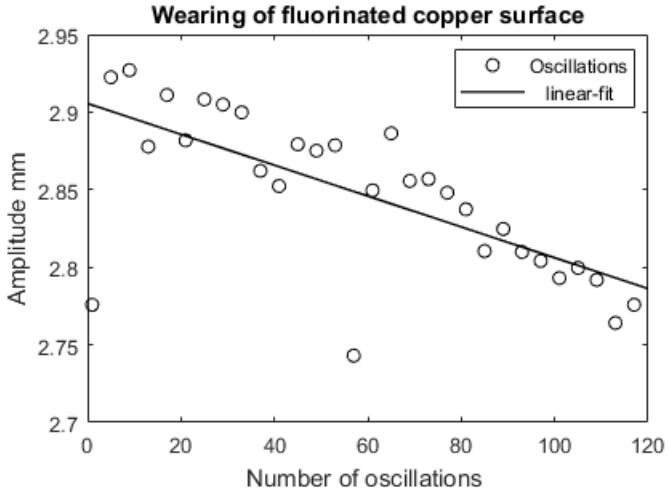

Figure 23: Wearing of the fluorinated copper surface by repeated oscillations of ferrofluid droplet.

6.5.2 Nanofilament surface

The second type of superhydrophobic surfaces used were nanofilament surfaces that has been grown by another research team [41]. Silicone nanofilament coatings are resistant to the mechanical stress and are chemically stable [42]. The nanofilaments are grown on top of silicon plate in a reaction of methyltrichchlorosilane (MTCS) and water. The degree of hydrophobicity that the nanofilament surface exhibits depends on proportions of the reactants. This mechanism makes it possible to produce nanofilament surfaces that range from extremely to just barely hydrophobic. The contact angles of the nanofilament surfaces used for this this thesis are in the table below.

Contact angles of nanofilament surfaces			
Surface	Advancing $\pm 3°$	Receding $\pm 2°$	Hysteresis $\pm 3.5°$
M90	173°	151°	22°
N04	173°	165°	8°
L12	178°	145°	33°
L29	164°	133°	31°
L28	161°	133°	28°
L22	167°	133°	34°
L20	168°	134°	34°

Synthesis of nanofilament surface

The silicone nanofilaments are grown on purified silicon wafers. The purification is a two step process where in the first step the silicon wafers are washed with de-ionized water and dried under nitrogen flow. The second step is purifying the surface further and activating it with oxygen plasma [41]. After cleaning the substrates are immediately placed in the in-house-build reaction chamber and surrounded by vacuum [41]. First de-ionized water and after that MTCS were let to evaporate through the inlet valve into the vacuum chamber [41]. The reaction of MTCS with hydroxyl groups of the silicon wafer surface causes the growth of nanofilaments. At the end of the reaction the by-products were removed from the chamber with nitrogen stream [41].

6.6 Data-analysis

The measurements are done by recording the position of ferrofluid droplet during the oscillations with high speed camera (Phantom Miro 310) and macro lens (Sigma 150mm f/2.8 APO Macro). Videos are then analyzed with custom matlab codes that find the position of the droplet frame-by-frame. For the successful analysis it is therefore important to have a good contrast between the droplet and background.

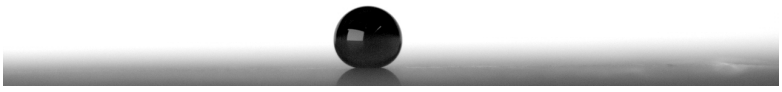

Figure 24: Droplet on a fluorinated copper-surface. Good contrast between the droplet and the background is achieved with extra lighting and white paper tissues that cover the vertical stage.

After a couple seconds of oscillation the droplet amplitude becomes constant. The steady-state amplitude means that energy losses due to dissipations equals to external energy brought to the system by magnet. Droplet is oscillated with different frequencies around its resonance peak and the amplitudes are compared to theoretical predictions.

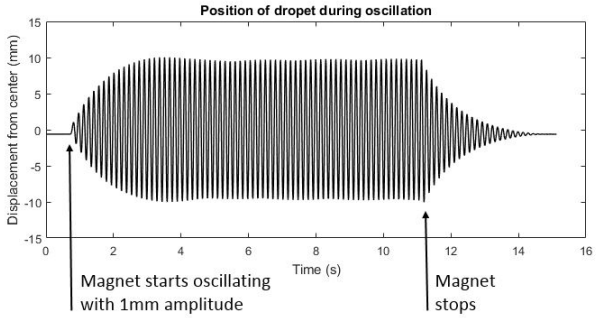

Figure 25: Position of the droplet during oscillations. Two magnets oscillate near droplet resonance with frequency of 6.6Hz and amplitude of 1mm. The droplets amplitude is a much larger than magnet amplitude.

Due to complexity of droplets movement, theoretical calculations are made by simulating the droplet movement on the surface with varying dissipational forces. The droplet oscillations are simluated with different frequencies near resonance. Comparing the theoretically obtained resonance peaks with the measured peaks on test surfaces makes it possible to extract the dissipations that are present during the measurements. In the previous research the viscous and frictional dissipations were successfully extracted by this method [14].

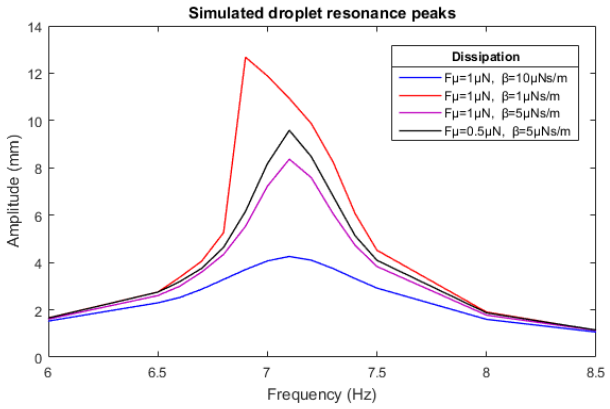

Figure 26: Theoretical calculations of the resonance peak for ferrofluid droplet with concentration of $0.2vol-\%$ oscillated by two largest magnets. The frictional dissipations affect primarily the height of peak and the position of it on the frequency scale is affected only slightly.

Chapter 7

Results and discussion

The objective of the project was to optimize the driven oscillator method to be applicable to a wide range of surfaces. The optimization is done by varying parameters throughout the measurements and finding their impact on resonance peak. Parameters varied are magnet size and separation, droplet volume and concentration of ferrofluid. Based on the results driving amplitude and frequency range is chosen.

7.1 Choosing a magnet

The magnet size was chosen from the three options described in materials and methods section. In the magnet choosing process the resonance peak for the $0.2vol-\%$ droplet were measured with the magnet separation of 30mm. First the measurements were done on the extremely superhydrophobic copper surface with three low-as-possible driving amplitudes. Resulting resonance peaks pictured in the figure 27.

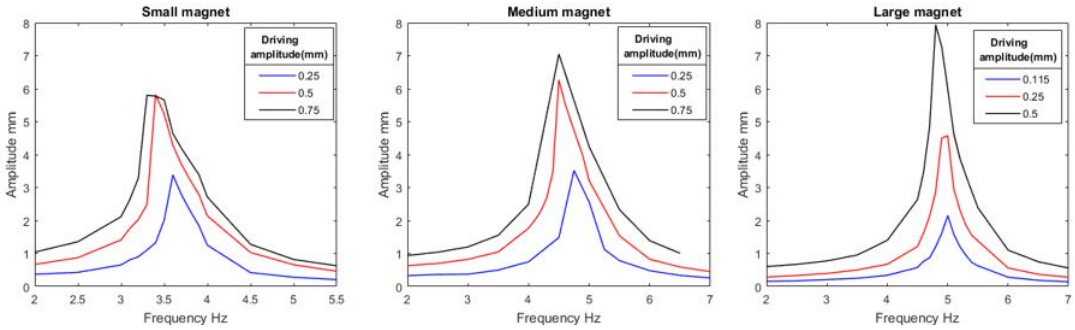

Figure 27: The resonance peaks of $5\mu l$ droplet with three different magnet sizes on the fluorinated copper surface. Ferrofluid concentration $c = 0.2vol-\%$ and separation of magnets $d = 30mm$.

From the figures it is notable that peaks are positioned at higher frequencies when the larger magnets are used for oscillations. This indicates stronger magnetization in the ferrofluid droplet due to increased magnetic field affecting it. A slight correlation is also noticeable between the peak position on frequency scale and the driving amplitude. This is likely caused by an increase in the magnet oscillation speed that forces the droplet to move faster as well.

The same measurements were then repeated on a less hydrophobic nanofilament surface (M90) with advancing contact angle of $173 \pm 3°$ and $22 \pm 3.5°$ hysteresis. The results of the measurements are in the figure 28.

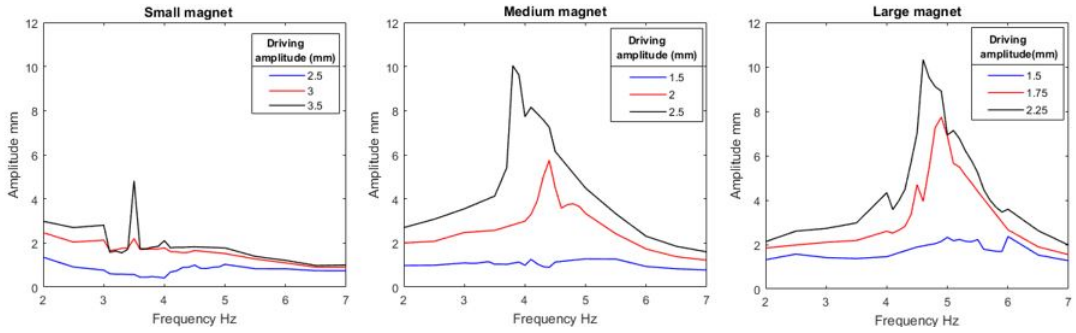

Figure 28: Repeated measurement of figure 27 on the nanofilament surface M90 with advancing contact angle of $173 \pm 3°$ and $22 \pm 3.5°$ hysteresis. The sudden valleys in the peaks are associated with the evaporation of the droplet during the measurement and possible contamination of surface. The peak smoothness in this case is not relevant since the goal was to roughly screen the lowest driving amplitudes of peak formation.

Looking at the figure 28 it is fairly obvious that the magnetization associated with the smallest of the magnets is not enough to move the droplet along the nanofilament surface and form a clear resonance peak. The options left are the medium sized magnet along with the largest size both of which have strong enough fields for moving the droplet. For the medium sized magnet the lowest driving amplitude with a clear resonance peak is $2.5mm$. Although, some peak formation is visible with the driving amplitude of $2mm$ the peak is not quite clear enough to be compared with the theoretical model. Driving the oscillations with the largest magnet leads resonance peak with the amplitude of $1.75mm$ which is much lower than in the case of medium magnet.

It is important for the driving amplitude to be as small as possible for a number of reasons. A small driving amplitude keeps the droplet amplitude smaller as well which enables a more precise characterization of the local surface properties.

Moreover, large magnet amplitudes also cause vibrations to the surroundings especially when the frequency is also high. Vibrations can reduce the reliability of the measurements by shaking the sample. For the same reason the frequency range should also be kept as low as possible.

Because of the smaller driving amplitude the largest magnet size is chosen to drive the oscillations in the prototype. The downside of the magnet choice is the higher frequencies needed to produce the resonance peak. Yet since the peak position is strongly associated with the ferrofluid magnetization it is more favorable to reduce the concentration of ferrofluid rather then the size of magnets.

7.2 Concentration of the ferrofluid

Because of dispersed nanoparticles, the viscosity of ferrofluid is slightly increased from that of pure water even with particle concentration of just $0.2\%_{vol}$ [14]. Ideally the particle concentration in the liquid should be as low as possible for the more water like properties. However, moving the droplet on the less hydrophobic surfaces requires considerably higher magnetization in the ferrofluid than when in the case of highly superhydrophobic surfaces.

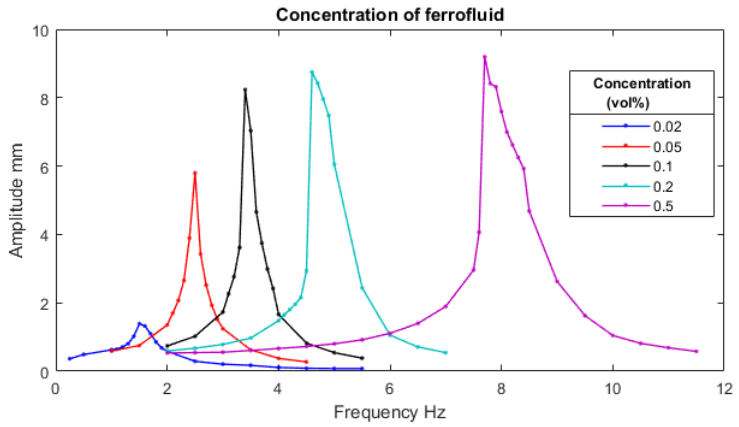

Figure 29: The effect of concentration on the resonance peaks. The position of the peak on frequency scale is moved to higher frequencies due to increased magnetization in a more concentrated ferrofluid droplet. Measurements done with largest magnets, separated by $d = 30mm$ and droplet volume of $5\mu l$.

The concentration of ferrofluid was varied between $0.02\%_{vol}$ and $0.5\%_{vol}$ while keeping the other parameters constant. The results in figure 29 show the peak position steadily moving onto the higher frequencies along with rapid increase in peak height when concentration is less than $0.1\%_{vol}$.

Choosing a small ferrofluid concentration would make sense in terms of liquid properties becoming more water-like. However, when trying to drive oscillations on nanofilament surfaces the ferrofluid concentration of $c = 0.1\%_{vol}$ was the lowest possible that was able to force movement in the droplet. The movement was achieved with the magnet driving amplitude as large as $2.5mm$ with the magnet separation of $20mm$. The driving amplitude could be reduced to $1.5mm$ by increasing the concentration to $c = 0.15\%_{vol}$.

7.3 Separation of magnets

The magnetization of the ferrofluid droplet is determined by the strength of magnetic field that is affecting it along with the concentration of fluid. When the separation of two magnets is small the magnetic field affecting the droplet becomes larger and the droplet moves along the surface more readily.

In our setup the lower of the magnets is fixed to the linear stage and for increasing the magnet separation the upper magnet is lifted. The position of the surface is controlled by the separate vertical stage that is also used to measure exact distance between magnets. The upper limit to the magnet separation comes from this stage and is $d_{max} = 50mm$. Lower limit for the separation is $d_{min} = 20mm$ that comes from practical issues that are associated with conducting experiments. The droplet is pipetted onto the surface between the magnets by hand and the gap too small would make droplet deposition difficult and increases the risk of damaging the surface with the tip of the pipette. The resonance peaks measured with the separation within these limits are pictured in the figure 30.

As expected, the resonance peak is found at higher frequencies when the separation of magnets is small. Position of the peak can be manipulated by changing magnet distance and ferrofluid concentration.

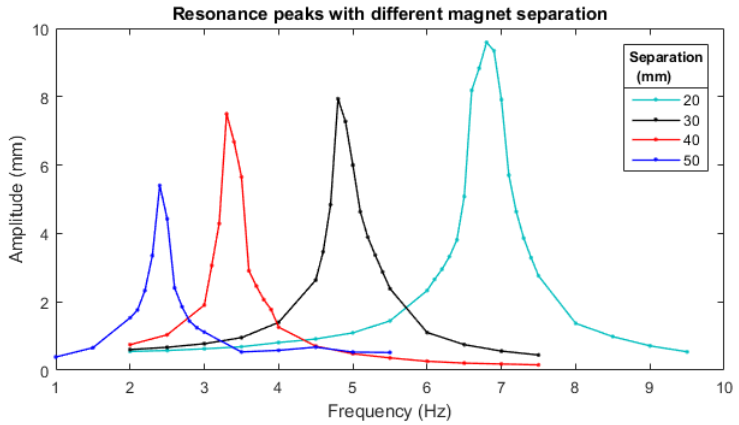

Figure 30: The resonance peaks on the copper surface with magnet separations of $20mm$, $30mm$, $40mm$ and $50mm$. Ferrofluid concentration is $0.2\%_{vol}$.

Connection to the concentration of ferrofluid

As previously explained it is most favorable to keep the ferrofluid concentration as low as possible. The same position for the resonance peak can be achieved by using both large separation of the magnets along with high concentration ferrofluid or on the contrary by small magnet separation together with low concentration ferrofluid. The less concentrated ferrofluid along with smaller magnet separation is the sensible solution. Choosing the smallest possible separation of magnets $d_{min} = 20mm$ along with $0.15\%_{vol}$ ferrofluid concentration leads to the peak position between $6.5Hz$ and $7.5Hz$.

7.4 Volume of droplet

Volume of the ferrofluid droplet was the last parameter to be optimized due to its lack of connection to other parameters. Increasing the volume of ferrofluid droplet does not affect peak position nor the shape of it. This was found by varying the droplet sizes between $2\mu l$ and $100\mu l$ in otherwise similar measurements. The measurements were successful only with three smallest droplet sizes $2\mu l$, $3\mu l$ and $4\mu l$ since they were the only ones with linear oscillations. The rest of the droplet sizes exhibited circular motions near resonance frequency (see figure 31 (right)). This causes the droplet to move from the camera focus and in some cases deformations in resonance peak shape. Therefore the frictional values from the

peak of circularly moving droplet contain some serious errors and those measurements can not be used for the wetting characterization purposes. The reasons for circular motions are discussed in the next sub-chapter.

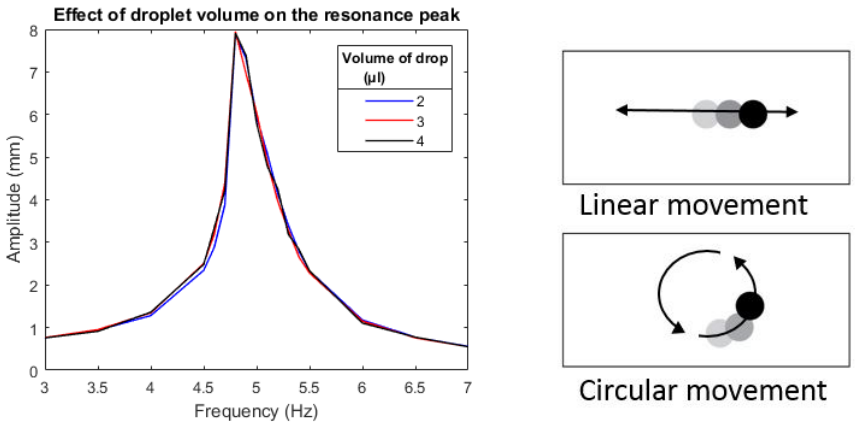

Figure 31: *Left subfigure:* Resonance peaks with different volume droplets. The peak is unaffected by the changes in droplet volume when the oscillation path is linear.
Right subfigure: The linear and circular droplet movements. When the droplet size is increased over $5\mu l$ it starts oscillating on circular path when oscillated near resonance frequency. Circular motions lead to errors in resonance peak.

From the three successful peak measurements shown in figure 31 is visible that the peaks are close to identical. That is expected since the height of peak is closely related to the frictional values of the surface, driving amplitude and volume magnetization. Since the ferrofluid is kept the same throughout the whole measurements ($c = 0.2\%_{vol}$) the volume magnetization in a droplet is the same as well. In theory the droplet size would be irrelevant for the purposes of building a prototype as long as it is in the range that oscillates linearly. In practice however it is the best to choose the larges droplet possible. In our case that is $4\mu l$.

The reason behind choosing the largest droplet is the fast evaporation of tiny droplet. The evaporation reduces mass of droplet and causes an increase in the ferrofluid concentration leading to higher volume magnetization. This increases the droplets resonance frequency and the resonance peak shifts to the right on the frequency scale as is shown in figure 29. The average measurement time is third of a minute somewhat depending on a frequency used and the amount on oscillations. From the figure 32 we can see that one minute time of waiting before oscillations is enough to create a measurable shift in the peak position. In a larger droplet the

surface-to-volume ratio is smaller making the effects of evaporation less significant. Using as large droplet as possible therefore reduces errors in the measurements.

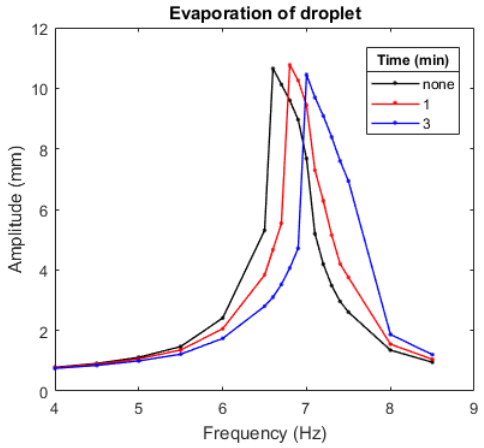

Figure 32: Evaporation of 5 μl ferrofluid droplet. Evaporation of water from the droplet increases the concentration of nanoparticles and the resonance peak is found at higher frequencies.

7.4.1 Circular droplet movement

The circular motions are only present in the two magnet system. They appear when the magnetization and volume of droplet is large enough and the driving amplitude exceeds over a certain threshold. One of the reasons for them could be deformation of the larger droplet due to rapid movements. In figure 33 is a picture series of 50 μl droplet during one half oscillation near its resonance frequency ($f = 6.3Hz$). For the large drop the deformation is clearly visible with bare eye. Such deformation were not noticeable in the smallest droplets during circular motions but they might be caused by smaller deformations that can not be detected without analysis tools.

In the figure 33 is visible that when droplet is at the end positions of oscillation it has more round shape and during the movement the drop is flattened against the surface. Since the circular motions appear only with the two magnet systems it is possible that the deformation moves the droplets centroid closer to one magnet than the other. This combined with misalignment of the magnets or a non-uniform magnetization in them creates unexpected forces that are driving the droplet onto circular path. For the smaller droplets deformation is not as significant since the surface to volume ratio is larger and the surface tension might be significant enough to overcome the deforming forces.

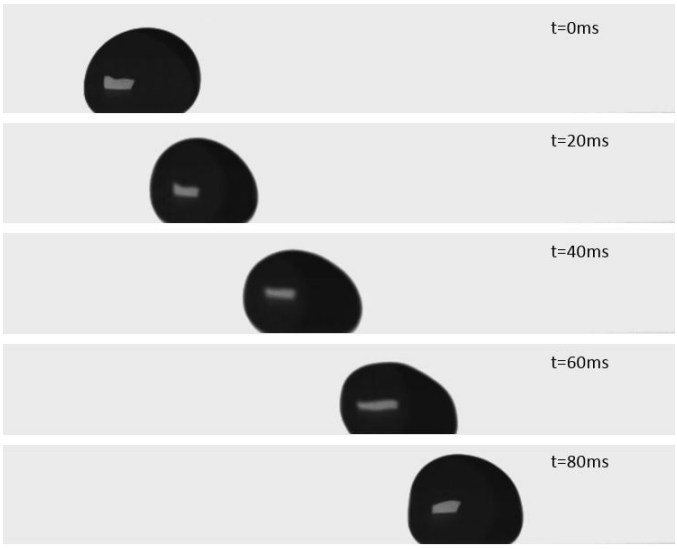

Figure 33: The deformation of $50\mu l$ droplet during half-oscillation close to its resonance frequency ($f = 6.3Hz$).

The idea of the droplet deformation being caused partly by its magnetization is supported by the more frequent occurrence of the circular motions with small magnet separation and high ferrofluid concentrations. However, it does not explain why circular motions only show up when the driving amplitude of the magnet is large enough. This might be explained by the forces driving the droplet on the circular path being correlated with droplet amplitude. With the amplitude being small the forces may not be enough to cause deformations in droplet shape. Interestingly, when measuring on the less hydrophobic surfaces circular motions were not as common despite larger amplitudes. The large friction of such surface may in those cases overcome the forces that drive the droplet on the circular path.

The round motions can be avoided also by other means than reducing the droplet volume. Shifting the droplet position closer to the lower magnet flattens the droplet and two magnet system start to resemble one magnet system where the round motions were absent. This might not bee a good solution since the frictional forces depend on the normal force [14]. Yet if the exact connection could be established between the normal force and measured surface friction the displacement of droplet from the center of magnets may be applicable.

Despite previous speculations, verified reason for the droplet moving on a circular path is not determined. Since it may be caused by the imperfections in our current setup it is sensible to repeat measurement with different droplet volumes with the

prototype when it is built and compare results before making a final decision on the size that is optimal.

7.5 Driving amplitude and driving frequency

The amplitude and frequency ranges are determined by other parameters. During the optimization process driving amplitudes and frequencies were considered and kept as small as possible. In the beginning of the project it was planned to have only one driving amplitude for the device due to the lower cost of such linear stage. Yet this would have limited the wetting characterization to only extreme hydrophobic surfaces. The less hydrophobic surfaces require larger driving amplitudes for the successful measurements. Based on the measurements pictured in figures 27-32 the suggested driving amplitude range for the magnets is $0.1mm - 2.5mm$. The needed frequency sweep range is $3Hz - 9Hz$ since in all of the cases with chosen parameters the peak is found within this frequency zone.

7.6 Measurements on nanofilament surfaces

For the precise wetting characterization it is important for the method to distinguish small differences in the wetting properties of surfaces. To get a sense of the methods precision four measurements were made on nanofilament surfaces that are similar but non-identical in their wetting properties. The measurements were done using parameters chosen in previous sections: Largest magnets with separation $d = 20mm$, droplet concentration $c = 0.15\%_{vol}$ and volume $V = 4\mu l$.

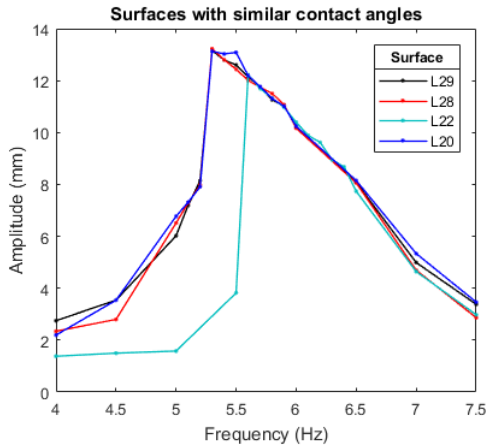

Contact angles		
Surface	Advancing ±3°	Hysteresis ±3.5°
L29	164°	31°
L28	161°	28°
L22	167°	34°
L20	168°	34°

Figure 34: Nanofilament surfaces with similar wetting properties.

In the figure 34 the measurement done on surface L22 stands out. The amplitude of droplet is considerably lower before the $5.5Hz$ frequency than in the other measurements. Likely the smaller amplitude is caused by contamination or non-homogeneity of the surface and is not associated directly with the measurement method. Despite measurement on L22 there is no notable difference between measurements on other surfaces. Including surfaces L20 and L28 with 6° difference in their contact angle hysteresis.

Partly the results in figure 34 may be caused by the difficulties associated with the sessile droplet contact angle measurements. Also it is possible that the nanofilaments on surfaces have grown non-homogeneously and the difference is because the oscillatory and sessile drop measurements are done at different locations. Other possible reason is the surface degeneration between two measurements since the sessile drop measurement has been preformed months prior to the oscillation measurement. Any combination of the causes mentioned above is possible as well. Further measurements are needed on the surfaces with similar properties before any justified conclusions can be made. That being said, it can not be excluded that the method may not be suitable for the wetting characterization of the surfaces with contact angles this low.

Comparing the measurements done on copper surface and the superhydrophobic nanofilament surface N04 (advancing contact angle $173 \pm 3°$ and hysteresis $8 \pm 3.5°$) a difference in resonance peaks can be detected. Hysteresis of copper surface is 3° smaller than of nanofilament surface N04. This is visible in the figure 35 as a slightly larger peak measured on the copper surface indicating lesser frictional forces.

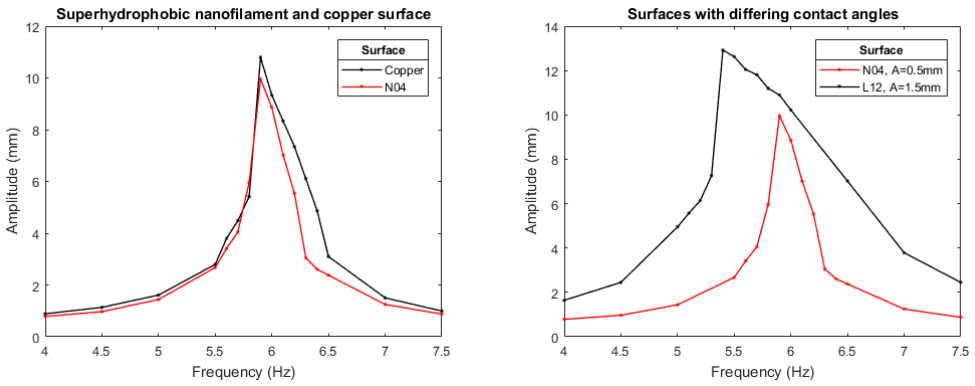

Figure 35: *Left subfigure:* The resonance peaks on copper surface and nanofilament surface N04 with same parameters. *Right subfigure:* The resonance peak of nanofilament surfaces N04 and L12. Same parameters were used with an exception of driving amplitude.

In the figure 35 is a resonance peak of N04 compared to the peak of the surface L12. The advancing contact angle is very high on both of the surfaces (advancing contact angle of L12 $178 \pm 3°$) but the hysteresis is considerably larger in L12 ($33 \pm 3.5°$). Because of the stronger adhesion of the droplet to L12 larger driving amplitudes were used while measuring. The difference in peak height is caused by driving amplitudes. From the figure 35 it can concluded that shape of peak is affected by contact angle hysteresis. Peaks measured on surfaces with large hysteresis are short and broad while those on superhydrophobic surfaces are high and narrow.

7.7 Compatibility of simulations with measurements

For the extraction of frictional forces that are inhibiting the droplet movement on surface measurements with chosen parameters were made and compared to the simulations with same parameters. Unexpectedly, the position of the peaks on frequency scale were higher in simulations. The results are shown in the figure 36. In left figure is the measurement and theoretical predictions for the resonance peak on copper surface. Likewise on the right figure is measurement and equivalent simulation for the surface L12. In both figures the shape of peaks are compatible but the measured peak is found at lower frequencies.

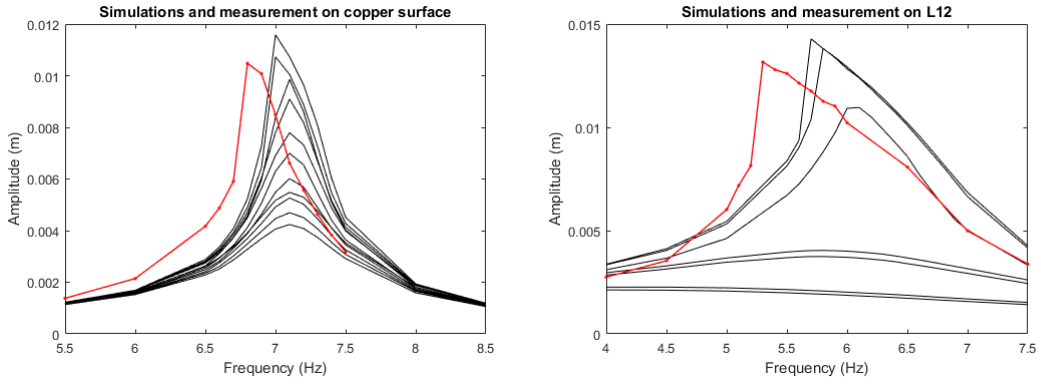

Figure 36: Measured and simulated resonance peaks on copper surface (left) and nanofilament surface (right). The measured peaks are found at lower frequencies than simulated. Ferrofluid concentration used was $c = 0.20\%_{vol}$ for copper and $c = 0.15\%_{vol}$ for nanofilament surface measurement.

The resonance peaks position is largely dependent on the droplet magnetization and the difference between the simulations and the measurements translates to

overestimation of magnetization in the droplet when simulating its movement. The simulation model in use is the same model used in the previous research of [14]. It is likely that some approximations which were accurate for a one magnet system have to be reconsidered when simulation the droplet movement driven by two magnets. One of the approximations made is that demagnetizing field inside the droplet is negligible. Demagnetizing fields are magnetic fields within that are anti-parallel to the magnetization direction [34]. Simplifying the droplet as a small magnet the magnetization direction of dipoles inside it are pointing at the north pole of magnet. The field direction is from north to south pole so that inside the droplet it is in opposite direction of magnetization. This reduces the magnetic field inside the drop and leads to smaller magnetization in ferrofluid.

In the previous research magnet size was smaller leading to droplet magnetization being smaller as well. With larger magnetization the demagnetizing field also increases and possibly can not be considered negligible anymore.

Despite the obvious difference in the peak location, the simulated peaks resemble measurements in the shape quite closely for both surfaces. This means that if the location of simulated peaks can be corrected by taking demagnetizing fields into account, frictional values can be extracted even from the less hydrophobic surfaces and the simulations will not be a limitation to the methods applicability.

Conclusions

This thesis presented the theoretical framework and the optimization process of the new method for characterizing wetting properties of superhydrophobic surfaces. The driven oscillatory method would seem to be applicable at least in superhydrophobic range. However, frictional forces could not be extracted from the measurements due to the disagreement with theoretical model. The difference may be caused by mismatch in magnetization of ferrofluid in a droplet due to simplifications used in simulation model. The first step would be to investigate the the effect demagnetizing fields have on peak location. In case the effect is large enough for simulations to be comparable with measurements the demagnetizing fields can be taken into account during the simulations.

If the effect of the demagnetizing fields is found to be negligible, some other possibilities could be considered as well. In the previous research [14] the magnetometer used for characterizing magnetic properties of ferrofluid has a different working principle. The SQUID (superconducting quantum interference device) -type magnetometers are more sensitive in measuring the sample magnetization than VSM [38]. By measuring the ferrofluid magnetization with SQUID could lead to different results in simulations.

The exact limitations of the method can be found only when theoretical model is compatible with experiments and frictional forces can be extracted. For finding limitations the method needs to be examined further on a variety of surfaces. In future it would be interesting to try it on other types of hydrophobic surfaces as well, like commercial coatings and textured surfaces.

Bibliography

[1] A. Marmur, "Soft contact: measurement and interpretation of contact angles", Soft Matter, vol. 2, pp. 12-17, 2006.

[2] N,J. Shirtcliffe, G. McHale, S. Atherton and M. I. Newton, "An introduction to superhydrophobicity", Advances in Colloid and Interface Science, vol. 161, pp. 124-138, 2010.

[3] H. K. Webb, R. J. Crawford, E. P. Ivanova, "Wettability of natural superhydrophobic surfaces", Advances in Colloid and Interface Science, vol. 210, pp. 58-64, 2014.

[4] N. J. Mlota, C. A. Toveyb and D. L. Hu, "Fire ants self-assemble into waterproof rafts to survive floods", Proceedings of the National Academy of Sciences of the United States of America, vol. 108, pp. 7669-7673, 2011.

[5] N. Valipour M, F. C. Birjandi and J. Sargolzaei, "Super-non-wettable surfaces: A review", Colloids and Surfaces A: Physicochemical and Engineering Aspects, vol. 448, pp. 93-106, 2014.

[6] C. Jin, Y. Jiang, T. Niu and J. Huang, "Cellulose-based material with amphiphobicity to inhibit bacterial adhesion by surface modification", Journal of Materials Chemistry, vol. 22 , pp. 12562–12567, 2012.

[7] M. Ma and R. M. Hill, "Superhydrophobic surfaces", Colloid and Interface Science, vol. 11, pp. 193-202, 2006.

[8] S. Shibuichi, T. Onda, N. Satoh and K. Tsujii, "Super Water-Repellent Surfaces Resulting from Fractal Structure", Journal of Physical Chemistry, vol. 100, pp. 19517-19517, 1996.

[9] C. Lee, C. Choi and C. J. Kim, "Superhydrophobic Drag Reduction in laminar flows: a critical review", Experiments in Fluids, vol. 57, pp. 176, 2016.

[10] M. He, J. Wang, H. Li, X. Jin, J. Wang, B. Liu and Y. Song, "Super-hydrophobic film retards frost formation", Soft Matter, vol. 6, pp. 2396-2399, 2010.

[11] X. Zhan, Y. Yan, Q. Zhang and F. Chen, "A novel superhydrophobic hybrid nanocomposite material prepared by surface-initiated AGET ATRP and its anti-icing properites", Journal Of Material Chemistry, vol. 2, pp. 9390-9399, 2014.

[12] D.Quere, "Wetting and Roughness", The Annual Review of Materials Research, vol. 38, 2008.

[13] C. Dorrer and J. Rühe, "Some thoughts on superhydrophobic wetting", Soft Matter, vol. 5, pp. 51-61, 2009.

[14] J. V. I. Timonen, M. Latikka, O. Ikkala, and R. H. A. Ras, "Free-decay and resonant methods for investigating the fundamental limit of superhydrophobicity," Nature Communications, vol. 4, 2013.

[15] A. Marmur, C. D. Volpe, S. Siboni, A. Amirfazli and J. W. Drelich, "Contact angles and wettability: towards common and accurate terminology", Surface Innovations, vol. 5, pp. 3-8, 2017.

[16] T. Young, "An essay on the cohesion of fluids", Philosophical Transactions of the Royal Society of London, vol. 95, pp. 65 – 87, 1805.

[17] G. Wolansky and A. Marmur, "The Actual Contact Angle on a Heterogeneous Rough Surface in Three Dimensions", Langmuir, vol. 14, pp. 5292-5297, 1998.

[18] K. Cheng, B. Naccarato, K. J. Kim and A. Kumar, "Theoretical consideration of contact angle hysteresis using surface-energy-minimization methods", International Journal of Heat and Mass Transfer, vol. 102, pp. 154-161, 2016.

[19] M. Nosonovsky and B. Bhushan, "Lotus Versus Rose: Biomimetic Surface Effects", Green Energy and Technology, vol. 49, pp. 25-40, 2012.

[20] D. Quéré, "Non-sticking drops", Reports on Progress in Physics, vol. 68 , pp. 2495-2532, 2005.

[21] P. Roura and J Fort, "Local thermodynamic derivation of Young's equation", Journal of Colloid and Interface Science, vol. 272, pp. 420-429, 2004.

[22] K. Seo, M. Kim and D. H. Kim, "Surface Energy: Re-derivation of Young's equation, Wenzel equation, and Cassie-Baxter equation based on energy minimization", InTech, 2015.

[23] M. J. Neeson, R. R. Dagastine, D. Y. C. Chanabe and R. F. Tabor, "Evaporation of a capillary bridge between a particle and a surface", Soft Matter, vol. 10, pp. 8489-8499. 2014.

[24] Y. Yuan and T. R. Lee, " Contact angle and wetting properties", Surface Science Techniques, vol. 51, pp. 3-34, 2013.

[25] T. S. Meiron, A. Marmur and I. S. Saguy, "Contact angle measurement on rough surfaces", Journal of Colloid and Interface Science, vol. 274, pp. 637-644, 2004.

[26] R. N. Wenzel, "Resistance of solid surfaces to wetting by water", Industrial and Engineering Chemistry, vol. 28, pp. 988-994, 1936.

[27] A. B. D. Cassie and S. Baxter, "Wettability of porous surfaces", Transactions of the Faraday Society, vol. 40, pp. 546-551, 1944.

[28] X. Dai, B. B. Stogin, S. Yang and T. S. Wong, "Slippery Wenzel State", ACS Nano, vol. 9, pp. 9260–9267, 2015.

[29] A. J. B. Milne and A. Amirfazli, "The Cassie equation: How it is meant to be used", Advances in Colloid and Interface Science, vol. 10, pp. 48-55, 2012.

[30] Y. Liu, X. Chen and J. H. Xin, "Hydrophobic duck feathers and their simulation on textile substrates for water repellent treatment", Bioinspiration and miomimetics, vol 3, 046007, 2008.

[31] B. Krasovitski and A. Marmur, "Drops Down the Hill: Theoretical Study of Limiting Contact Angles and the Hysteresis Range on a Tilted Plate", Langmuir, vol. 21, pp. 3881-3885, 2005.

[32] N. Wu, J. Dai and F. J. Micale, "Dynamic Surface Tension Measurement with a Dynamic Wilhelmy Plate Technique", Journal of Colloid and Interface Science, vol. 215, pp. 258–269, 1999.

[33] I. A. Larmour, S. E. J. Bell and G. C. Saunders, "Remarkably Simple Fabrication of Superhydrophobic Surfaces Using Electroless Galvanic Deposition", Angewandte Chemie International Edition, vol. 46, pp. 1710-1712, 2007.

[34] J. M. D. Coey, "Magnetism and magnetic materials", Cambridge University Press, 2009.

[35] Occultopedia, L, Lodestone, http://www.occultopedia.com/l/loadstone.htm Retrieved on 7.9.2017.

[36] V. V. Mody, A. Singh and B. Wesley, "Basics of magnetic nanoparticles for their application in the field of magnetic fluid hyperthermia", European Journal of Nanomedicine, vol. 5, pp. 11-21, 2013.

[37] K&J Magnetics Inc, "Why are most neodymium magnets plated or coated?", https://www.kjmagnetics.com/FAQ.asp. Retrieved on 8.9.2017.

[38] Z. Boekelheide and C. L. Dennis, "Artifacts in magnetic measurements of fluid samples", Journal of Applied Physics, vol 6, 08521, 2016.

[39] R. L. Rebodos and P. J. Vikesland, "Effects of Oxidation on the Magnetization of Nanoparticulate Magnetite", Langmuir, vol. 26, pp. 16745–16753, 2010

[40] N. S. S. Mousavi, S. D. Khapli, and S. Kumar, "Direct observations of field-induced assemblies in magnetite ferrofluids", Journal of Applied Physics, vol 117, 103907, 2015.

[41] J. T. Korhonen, T. Huhtamäki, T. Verho and R. H. A. Ras, "Hollow polysiloxane nanostructures based on pressure-induced film expansion", vol 2, pp. 116-126, 2014.

[42] T. Verho, C. Bower, P. Andrew, S. Franssila, O. Ikkala and R. H. A. Ras, "Mechanically Durable Superhydrophobic Surfaces", Advanced Materials, vol 23, pp. 673–678, 2010.